AD

Reports Control Symbol
OSD - 1366

TR-0309

UNIFIED VERY LOW STRATUS CLOUD/SUBCLOUD MICROPHYSICS MODEL

April 1992

Henry Rachele
U.S. Army Atmospheric Sciences Laboratory
White Sands Missile Range, New Mexico

Neal H. Kilmer
Physical Science Laboratory
Las Cruces, New Mexico

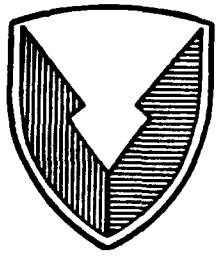

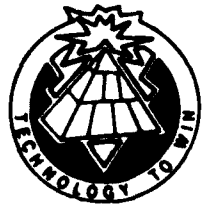

US ARMY
LABORATORY COMMAND
ATMOSPHERIC SCIENCES LABORATORY
White Sands Missile Range, NM 88002-5501

NOTICES

Disclaimers

The findings in this report are not to be construed as an official Department of the Army position, unless so designated by other authorized documents.

The citation of trade names and names of manufacturers in this report is not to be construed as official Government indorsement or approval of commercial products or services referenced herein.

Destruction Notice

When this document is no longer needed, destroy it by any method that will prevent disclosure of its contents or reconstruction of the document.

REPORT DOCUMENTATION PAGE

Form Approved
OMB No 0704-0188

1. AGENCY USE ONLY (Leave blank)	2. REPORT DATE	3. REPORT TYPE AND DATES COVERED
	April 1992	Final

4. TITLE AND SUBTITLE
UNIFIED VERY LOW STRATUS CLOUD/SUBCLOUD MICROPHYSICS MODEL

5. FUNDING NUMBERS
61102/B53A/B

6. AUTHOR(S)
Henry Rachele

7. PERFORMING ORGANIZATION NAME(S) AND ADDRESS(ES)
U.S. Army Atmospheric Sciences Laboratory
White Sands Missile Range, NM 88002-5501

8. PERFORMING ORGANIZATION REPORT NUMBER
ASL-TR-0309

9. SPONSORING MONITORING AGENCY NAME(S) AND ADDRESS(ES)
U.S. Army Laboratory Command
Adelphi, MD 20783-1145

10. SPONSORING/MONITORING AGENCY REPORT NUMBER

11. SUPPLEMENTARY NOTES

12a. DISTRIBUTION AVAILABILITY STATEMENT
Approved for public release; distribution is unlimited.

12b. DISTRIBUTION CODE

13. ABSTRACT (Maximum 200 words)

A model is presented for simulating very low stratus clouds and their associated subcloud regions. This model is based on the assumption that the atmosphere contains particles that can be chemically and physically characterized and that grow in the presence of moisture as a function of relative humidity, temperature, and the size and chemistry of the particles. Components of this model include droplet growth and evaporation, phase change and mass balance of total water, thermodynamics, and ascent of a cluster of drops enclosed in moist air. The model requires only limited user input: some conventional meteorological values at a reference height (2 m above ground level) and some parameter values and other specifications. Input values for a visibility parameter and relative humidity are used with a choice of air mass type to define the parameters of a truncated bimodal lognormal drop size distribution at the reference height. Vertical profiles of drop size distributions can be simulated and used for further analysis. Examples are shown for modeled vertical profiles of lapse rate, temperature, potential temperature, mass loading, relative humidity, drop size, and drop concentration.

14. SUBJECT TERMS	15. NUMBER OF PAGES
drop size distributions, extinction, haze, liquid water content, stratus clouds, theoretical model, vertical variation, vertical structure	72
	16. PRICE CODE

17. SECURITY CLASSIFICATION OF REPORT	18. SECURITY CLASSIFICATION OF THIS PAGE	19. SECURITY CLASSIFICATION OF ABSTRACT	20. LIMITATION OF ABSTRACT
Unclassified	Unclassified	Unclassified	SAR

NSN 7540-01-280-5500

Standard Form 298 (Rev 2-89)
Prescribed by ANSI Std 239-18
298-102

DEDICATION

This report is dedicated to the memory of Dr. Louis D. Duncan of the U.S. Army Atmospheric Sciences Laboratory. He not only encouraged the work but also willingly and enthusiastically gave many hours of his time discussing results and offering suggestions.

Accession For	
NTIS GRA&I	☑
DTIC TAB	☐
Unannounced	☐
Justification	
By	
Distribution/	
Availability Codes	
Dist	Avail and/or Special
A-1	

PREFACE

The purpose of this study was to determine if it were possible to construct a theoretically based model that could produce "reasonable" vertical profiles of drop size distributions and associated atmospheric parameters in very low stratus clouds and their associated subcloud regions and at the same time have a complexity somewhere between the "simple" empirical model currently used by the U.S. Army and highly complex academic level models. Moreover, the inputs required to solve the highly nonlinear equations that characterize the model would consist of a small number of ground level (2 m) conventional atmospheric observations, that is, no vertical profile measurements would be necessary. Finally, the model design should be simple enough to be executable on a comparatively small computer.

The overall approach (in an attempt to accomplish the above) is nontraditional for very low stratus clouds and, consequently, has become controversial. There are those who feel that the physics and thermodynamics of rising clusters of droplets are not appropriate for the vertical structuring of low stratus clouds. However, results to date from the model are so encouraging that I feel it must be a good analog for constructing the vertical structure of very low stratus clouds.

There are others, including the coauthor of this report, who insist that I am trying to get too much out of the model; it has been overextended. These extensions are driven by application needs, and I feel they will provide the ballpark estimates required.

As for the equations used in the model, some are well founded in the literature, others are nothing more than modern updates of those used in the past, and some are of our design. Finally, some ideas and constraints are based on my interpretations of relatively recent approaches and results by other authors.

Henry Rachele

CONTENTS

LIST OF FIGURES

LIST OF TABLES

Table **Page**

SYMBOLS

a = surface tension constant = 0.153 dynes/cm K (in equation (15))
a = temperature radiation constant (when used in lapse rate equation)
a_j = constant coefficient in polynomial
A = a double exponential constant (in equation (2))
A = coefficient defined by equation (55a) (except in equation (2))
A_C = net radiation effect in the cloud = an unknown function of z
A_W = activity of water ($A_W = f_r$ when $\delta = 1$) = $\exp(-\eta/(M_W/M_d))$
A_{W_t} = threshold water activity
B = a double exponential constant (in equation (2))
B = coefficient defined by equation (55b) (except in equation (2))
b = surface tension constant depending on water soluble substance (in equation (15))
b = an adjustable parameter related to "vertical" entrainment from layer above cloud top (when used in lapse rate equation)
c = an adjustable parameter related to "vertical" entrainment from layer above cloud top (when used in lapse rate equation)
C = a double exponential constant (in equation (2))
C = lumped value defined by equation (55c) (except in equation (2))
C_p = specific heat of dry air at constant pressure
C_{pG} = specific heat of water vapor at constant pressure
C_p^* = weighted sum of specific heats as defined by equation (22f)
D = lumped quantity defined by equations (27c) and (55d)
D_V = diffusion coefficient
E = Contribution of "horizontal" entrainment to dT/dz in cluster sphere (in equations (22a) and (22b))
E = force necessary to accelerate the mass being entrained per unit of total mass in sphere (in equations (35) and (38))
e_s = partial pressure of water vapor at saturation
e_v = partial pressure of water vapor
F_d = drag force per gram of mass in sphere
f = relative humidity of the ambient air
f_r = relative humidity of the air at the droplet surface
f_t = relative humidity of the ambient air at $(z - \Delta z)$
f_{rt} = relative humidity of the air at the droplet surface at $(z - \Delta z)$
g = acceleration due to gravity
G = $\partial(\ln f_r)/\partial r$ when f_r is defined by a modified form of a Hänel droplet growth equation
H = $-\partial(\ln f_r)/\partial T$ when f_r is defined by a modified form of a Hänel droplet growth equation
K = coefficient of heat conduction or exchange coefficient
k_t = mixing rate for momentum

k_z = mixing rate for heat

L_e = specific enthalpy of vaporization of water

m = mass of sphere

m_d = mass of dry particle material

m_s = mass of solute

M_s = molar mass of solute

m_w = mass of water

M_w = molar mass of water

$\frac{m_w}{m_d}$ = mass of water condensed on the particle per unit mass of dry material

$n(r)$ = number density of particles of radius r

$N(r)$ = the cumulative number density of particles of radius r

N_{ccn} = concentration of cloud condensation nuclei

N_i = number of droplets of size class i per cubic centimeter (i = 1, 2, . . .) (except in equation (53))

N_i = the number density corresponding with mode i of a bimodal distribution (in equation (53))

N_{ir} = N_i (number of droplets of size class i per cubic centimeter) at the reference height

n_s = number of moles of dry solute

N_{sc} = number of droplet size classes

n_w = mole number of water

P = $P_d + e_v$ = total pressure

P_d = partial pressure of dry air

q = specific humidity

r = droplet radius

r_d = initial dry particle radius, r(f = 0)

r_{di} = r_d for size class i

r_i = radius of droplet in size class i (i = 1, 2, . . .) (except in equation (53))

r_i = the mode radius for mode i of a bimodal distribution (in equation (53))

R = radius of cluster sphere

R_v = specific gas constant for water vapor

R_d = specific gas constant for dry air

S_L = specific heat of liquid water

S_{si} = specific heat of solid or dissolved substance i

$S_{v,w}$ = supersaturation

t = time

T = temperature of cluster in °K

T' = temperature of the ambient air in °K

T_0 = standard temperature (273.16 K)

T_r = temperature of the cluster in °K at the reference height

T_r' = temperature of the ambient air in °K at the reference height

ν = number of moles of ions formed from one mole of solute
v_w = specific volume of pure water
w = effective ascent rate of the ascending cluster
w_r = reference level value of w
$\dot{w}$ = vertical acceleration of cluster
W_C = grams of condensed matter per gram of dry air
W_L = grams of liquid water per gram of dry air
W_{si} = grams of solid or dissolved substance i per gram of dry air
W_v = grams of water vapor per gram of dry air = mixing ratio for water vapor
Υ = expression defined by equations (33) and (55e)
z = height above ground level
z_r = reference height (2 m)
Δz = height step size in numerical integration
α_e = entrainment parameter
ε = ratio of the molecular weight of water to the mean molecular weight of dry air = 0.621972
η = exponential mass increase coefficient
η^o = value of η at infinite dilution
θ_m = potential temperature for damp air
ρ = total mass in sphere divided by volume of sphere
ρ_a = density of dry air
ρ_{ar} = density of dry air at reference height
ρ_d = density of dry particle
ρ_w = density of pure water
ρ' = density of ambient damp air
σ = surface tension of a droplet
σ_e = extinction coefficient
σ_i = the standard deviation for mode i of a bimodal distribution
σ_{wo} = surface tension of pure water at standard temperature
Φ = practical osmotic coefficient
δ = curvature correction
δ_t = $\delta(A_{w_t})$ = curvature correction when water activity is at the threshold value
$\overline{A}, \overline{B}, \overline{C}$ = parameters in Hänel and Lehmann's approximation equation for the exponential mass increase coefficient

A prime (') is used to indicate an environmental quantity (i.e., outside of sphere). (a' and b' are exceptions to this statement.)

1. INTRODUCTION

The Army has a need to assess the effects of the atmosphere on the performance of modern sophisticated weapons and surveillance systems that employ electro-optical (EO) sensors. These atmospheric effects assessments are used by people involved in research, analyses, weapons design, wargaming, deployment, and tactics. Of particular interest is the ability of a sensor to "see" a target along slant paths through the lowest kilometer of the atmosphere, especially when moisture in the form of damp haze, fog, or low clouds is present. To assess the slant path effects, one requires knowledge of the vertical variations of the physical quantities of these moist environments, and especially the drop size distribution. These characteristics are currently obtained from models that are based on field data; that is, they are empirical. These models generally satisfy three user preferences: first the models must be as simple as possible, but produce "reasonable" results; second, the models can be initialized with a minimum number of surface data inputs, and third, the models should not be computer intensive.

The purpose of this study was to develop a theoretically based model to augment or replace the empirical models and also satisfy the user needs and preferences mentioned above. In particular, we wanted a model that would yield vertical profiles of drop size distributions that can be used to obtain acceptable estimates of vertical profiles of extinction, backscatter, and absorption in very low stratus clouds and their associated subcloud regions. (Very low clouds are considered to be clouds having bases less than 300 m above ground level. The subcloud region is the region between ground level and the base of the cloud.) In addition to simulating vertical profiles of drop size distributions, the model also produces profiles of temperature, pressure, relative humidity, specific humidity, mixing ratio, supersaturation, liquid water content (LWC), potential temperature, and density. There will be a user's guide (Kilmer, 1992) for this model.

The report is arranged as follows. First, we provide a brief background history and motivation for the model. This is followed by a description of the model concept, a listing of assumptions, model equations, model results including comparisons with field data, and a summary and conclusions. A list of symbols appears at the beginning of the text.

2. BACKGROUND

In the late 1970's the Army realized that the vertical characteristics of fog and very low stratiform clouds were not sufficiently well characterized for EO studies. As such, field data were collected during periods of fog and low stratus clouds in Germany and England in the late 70's and early 80's. Each set of data consisted of vertical profiles of drop size and drop number values obtained with Knollenberg FSSP-100 sensors attached to balloons that ascended and descended through the fogs and clouds. Typical LWC profiles derived from these data are shown in figure 1; profiles of extinction are shown in figure 2. Note that, in the portion of these figures below the maximum mass loading and extinction, the lower parts of the curves are concave downward; whereas the upper parts are convex. Some researchers define the base of the cloud as that height where the inflection of log (LWC) versus height curves occurs as shown by the dashed lines in figure 1. We have followed this definition in the examples modeled for this report.

The first set of data collected for research purposes consisted of seven profiles of drop size and drop number in the vicinity of Grafenwöhr, Germany (1976), and seven profiles from Meppen, Germany (1978). These data were reported by Duncan et al. (1980). The

range of drop radii recorded was 0.25 to 23.5 μm. A second set (89 profiles of the same size range) was measured at Meppen in 1980 as reported by Lindberg (1982). A third set (5 profiles of drop radii 0.2 to 50 μm) was taken at Cardington, England, in 1983 (Lindberg et al., 1984). The data from Germany were generally characteristic of very low stratus clouds; whereas those from England were obtained from higher clouds.

The first set of data from Germany was used (Duncan et al., 1980) to generate the basic empirical model as follows. The logarithm of LWC or extinction (σ_e) for each of three wavelengths (0.55, 4.0, and 10.6 μm) at each height z + 20 m was plotted against the logarithm of LWC or σ_e at height z, producing linear relationships, examples of which are shown in figures 3 and 4. A mathematical representation of figures 3 and 4 is

$$x(z + 20\,m) = a'x(z) + b' \tag{1}$$

where

$x(z + 20\,m)$ = ln LWC or σ_e at height z + 20 m

$x(z)$ = ln LWC or σ_e at z

a′ and b′ are empirical coefficients. This model is very appealing to the user since it is simple, very easy to execute, and requires only a single value of LWC or σ_e near the surface (2 m above ground) as input.

Heaps (1982) and Rachele and Kilmer (1991), in addition, showed that equation (1) can be expressed in double exponential form, that is,

$$\text{LWC or } \sigma_e = A \exp \{ B \exp Cz \} \tag{2a}$$

where z is expressed in meters. A, B, and C are related to a′ and b′ from equation (1) according to

$$A = \exp\left[\frac{b'}{1 - a'} \right] \tag{2b}$$

$$B = \left(\ln y_r + \frac{b'}{a' - 1} \right) (a')^{-z_r/20} \tag{2c}$$

$$C = \frac{1}{20} \ln a' \tag{2d}$$

and y_r is the value of LWC or σ_e at a reference height $z = z_r$, that is,

$$y_r \equiv \text{LWC}(z_r) \text{ or } \sigma_e(z_r) \tag{2e}$$

Heaps[1] also found that the Meppen 80 and Cardington cloud data yielded profiles that are generally consistent with Duncan's earlier results, except that the Cardington data seemed to show a discontinuity at the base of the cloud. Lindberg and Duncan (1985) provided adjustments to earlier models to account for the discontinuity between cloud and subcloud regions for the higher cloud cases.

The LWC and extinction models of Duncan and Heaps are basically empirical models representing the "average" profiles for the locales where the data were collected. In con-

---

[1] verbal conversation

trast, we are hopeful that the physical model developed in this report will be general enough to provide "reasonable" profiles for worldwide applications, while at the same time showing why one could expect considerable variation in drop size, extinction, and LWC profiles on a worldwide basis.

3. MODEL CONCEPT AND ASSUMPTIONS

Our current concept of this model envisions an ambient atmosphere that is characterized by the dynamics of its mean motion as modified by its turbulent elements, but has reached a steady state and is horizontally homogeneous. Imbedded in this ambient atmosphere is a layer of very low stratus clouds. We assume that the cloud layer is capped by an inversion layer. In addition, we also envision an element of air near the ground surface having a density sufficiently less than the ambient air to rise through the ambient air up to the top of the cloud. We refer to this element of air as a representative element. Other elements also exist, but they may either overshoot or undershoot the cloud top height. Of all the elements present, we focus only on the representative element in this model in an attempt to quantify the physical and thermodynamic changes that take place in the element as it rises. Imbedded in this representative element of air is a population of droplets. We refer to this combination of air, moisture, and droplets as a droplet cluster, or cluster of drops. We define and use the model equations in a way that characterizes the ambient atmosphere by imposing constraints that we feel are reasonable. The most rigid constraint requires that the model equations can be specified by using a small set of conventional input data obtained at a ground level reference height (say 2 m)–no profile data are required.

The initial drops of the cluster are characterized by the reference level drop size distribution; but as the cluster rises the drops change in size, and therefore the distribution changes. The physical and thermodynamical changes of the drops and their environment are computed as though a hypothetical completely permeable sphere envelops the drops and their environment. Hereafter, the terms cluster and sphere are used to include the drops and their environment. The environment outside the sphere is the ambient environment.

The model allows ambient air to enter the sphere as it ascends. This process is called entrainment (Rogers, 1979; Pruppacher and Klett, 1978, 1980). Also included in the current model is the loss of water (vapor only) from the sphere by a process we call shedding in the present work. This is consistent with our notion that as ambient air is mixed into the sphere, we also have air in the sphere diffused into the ambient environment. That is, part of the moisture component of the drop environment is shed into the ambient air as the cluster rises through the ambient environment. Hence, not only is ambient air being entrained into the cluster, but cluster air is also being transferred (shed) simultaneously out of the sphere into the ambient air.

The layer from the base of the cloud to the user input value for the top of the cloud is defined as the cloud layer. The base of the cloud is defined as the lowest point at which the cluster environment is saturated or the point of inflection on the log (LWC) versus height curve. In cases where there are such a large number of such hygroscopic nuclei that saturation is never reached or is delayed considerably beyond what would reasonably be considered the base of the cloud, the latter definition is useful.

The microphysics of the cluster environment is computed for that stage when the cluster environment is still distinguishable from the ambient environment. After an initial stage of cloud development, the cluster and ambient environments become indistinguishable from a practical measurement standpoint. At this stage we say that the cloud is in a mature state, and the cloud and subcloud regions are in steady state.

The model is purposely designed to require a minimum number of reference level inputs (standard observations) and a knowledge of the drop size distribution at the reference height, and the chemistry of the dry particles upon which moisture is condensed. We found, however, that an estimate of the cloud top height was also required.

The droplets comprising the cluster change in size with height in accordance with diffusion controlled differential equations—the smallest remaining in approximate equilibrium with their environment and the largest in nonequilibrium. Diffusion of water vapor through air always occurs from regions of higher relative humidity to regions of lower relative humidity, regardless of the relationship between a drop's radius and its critical supersaturation value.

The ascent rate of the cluster is affected by buoyancy, mass of liquid water, entrainment, and/or forced vertical lifting. The cluster stops rising in the vicinity of the top of the cloud.

The ambient and cluster environments have the same relative humidity. This assumption is used to relate the water vapor mixing ratio in the ambient environment to that in the cluster sphere.

The temperature difference between the cluster and ambient environments decreases linearly with height and is zero at the top of the cloud.

The ambient environment is damp and nonadiabatic.

The drop size distribution at the reference height is defined by Shettle and Fenn (1979) and is a function of relative humidity, visibility, and geography (urban, rural, maritime). However, droplets having dry radii less than a "lower cutoff" value set by the modeler are omitted.

The chemistry of the dry particles (condensation nuclei) is adequately characterized by Hänel and Lehmann (1981).

The equilibrium size of a drop is properly defined by Hänel and Lehmann (1981).

The cloud and subcloud regions are connected, and hence can be unified, for clouds whose bases are less than 300 m above the ground.

All droplets are in equilibrium with their environment inside the sphere at the reference height.

The volume of the sphere that envelops the droplets is equal to the total mass of dry air inside the sphere divided by the density of this dry air. The total masses of dry air and water vapor inside the sphere are affected by entrainment and shedding. The density of dry air depends on its partial pressure and the temperature according to the ideal gas law.

The total pressure of damp air at a given height is the same inside and outside the sphere. The vertical gradient of this total pressure obeys the hydrostatic approximation applied to damp air (dry air plus water vapor) in the environment. Since the water vapor mixing ratio inside the sphere may be different from the ambient environmental value, the partial pressures of dry air and water vapor inside the sphere may differ from the corresponding values outside the sphere.

The concentration of drops in a given size class is inversely proportional to the volume of the sphere.

4. FORMULATIONS

4.1 Equilibrium Drop Size Model (Hänel)

In this section we present a brief summary of the basic formulations that relate the size of a droplet to the relative humidity and temperature of its immediate environment, and the chemical composition of the drop, assuming that the drop is in thermodynamic equilibrium with its environment. For more detail one should read Hänel (1976), who initiates his development with the statement that his model is based on an equation that describes the influence of curvature and dissolved material on the equilibrium partial vapor pressure P_r over an uncharged particle. He also states that according to Harrison (1965) it is necessary to relate P_r to the equilibrium partial vapor pressure P_w over a plane surface of water being saturated with dry air. P_w is calculated for the total pressure P of the moist air surrounding the particle and for the particle's absolute temperature T.

After some discussion Hänel concludes that the ratio of P_r to P_w can be written as

$$\frac{P_r}{P_w} = A_w \exp\left(\frac{2\sigma v_w}{rR_vT}\right) \tag{3}$$

where A_w is the water activity of the particle's liquid cover with a hypothetical plane surface in absence of dry air in the gaseous as well as the liquid state, and can be measured within a closed laboratory system at well-defined equilibrium vapor pressure of water and temperature. Also, in equation (3), σ is the surface tension on the particle's surface, v_w the specific volume of pure water at the standard pressure of 1 bar, r the radius of curvature of the particle surface, and R_v is the specific gas constant of pure water.

The exponent part of equation (3) represents the curvature correction part of the pressure ratio when enough water is present to form a complete shell such that the drop can be regarded as a sphere. This curvature correction is written in abbreviated form as

$$\delta = \exp\left(\frac{2\sigma v_w}{R_vTr}\right) \tag{4}$$

Following Hänel and Lehmann (1981), two other cases also are considered for curvature correction: (1) a particle that does not have a complete liquid cover and may be nonspherical (expected at the smallest relative humidities), and (2) a particle in a transition region between the two extreme cases. The three cases are combined in the following formulation:

$$\delta = \begin{cases} 1 \text{ for } 0 \le A_w \le \dfrac{A_{w_t}}{\delta_t} \\ \delta_t \dfrac{A_w}{A_{w_t}} \text{ for } \dfrac{A_{w_t}}{\delta_t} < A_w < A_{w_t} \\ \exp\left(\dfrac{2\sigma}{\rho_w R_v T r} \right) \text{ for } A_{w_t} \le A_w \le 1 \end{cases} \tag{5}$$

Assuming that the particle is in thermodynamic equilibrium with the surrounding moist air, Hänel concludes that the ratio P_r/P_w of equation (3) is equivalent to the relative humidity f of the moist air; that is,

$$f = P_r/P_w \tag{6}$$

and, hence, f relates to A_W and δ as

$$f = A_w\delta \tag{7}$$

which, in the case of a plane surface, reduces to

$$f = A_w \tag{8}$$

At this point it is appropriate to discuss the form and characteristics of A_W. Hänel states that for the ideal case of a pure solute, that is, the particle is an aqueous solution of a pure solute, A_W can be written in four different equation forms. For our work we selected the exponential form

$$A_w = \exp\left(-\phi v \frac{n_s}{n_w} \right) \tag{9}$$

where ϕ is the practical osmotic coefficient; v the number of moles of ions formed from one mole of solute, being equal to 1 if there is no dissociation of the solute molecules; n_s the number of moles of the dry solute; and n_w is the mole number of water.

Since $n_w = m_w/M_w$ and $n_s = m_s/M_s$, where m_w is the mass of water, M_w its molar mass, m_s the mass of the solute, and M_s its molar mass, equation (9) becomes

$$A_w = \exp\left(-\phi v \frac{M_w}{M_s} \frac{m_s}{m_w} \right) \tag{10}$$

Defining $\phi v \dfrac{M_w}{M_s}$ as η_s, which can be described empirically, equation (10) is written as

$$A_w = \exp\left(-\eta_s \frac{m_s}{m_w} \right) \tag{11}$$

η_s is defined as the exponential mass increase coefficient.

For aerosol particles under real conditions of water uptake, Hänel writes equation (11) as

$$A_w = \exp\left(-\eta \frac{m_o}{m_w} \right) \tag{12}$$

where $m_o = m_u + m_s$ = total mass of a dry particle
m_u = mass of insoluble material
m_s = mass of the dry mixed solute

The exponential mass increase coefficient η is evaluated by using an expression that is a modification by Kilmer suggested by Hänel as a result of studies by Fitzgerald et al. (1982); that is,

$$\eta = \eta^o \left\{ 1 + \sum_{j=1}^{6} a_j \left(\frac{r_d}{r} \right)^j \right\} \tag{13}$$

where the polynomial coefficients a_j are determined by curve fitting combined data from Hänel and Lehmann (1981). The summation in braces thus represents a second order effect for the collection of all measurements.

The combined data used in curve fitting include two categories of data for each of the 10 samples reported by Hänel and Lehmann (1981): (1) discrete data for $A_w \leq 0.965$ and (2) values calculated for $0.965 \leq A_w \leq 1$ from Hänel and Lehmann's approximate extrapolation formula; that is,

$$\eta = \eta^o - \bar{A}\left(\frac{m_w}{m_d} \right)^{-1/2} + \bar{B}\left(\frac{m_w}{m_d} \right)^{-1} - \bar{C}\left(\frac{m_w}{m_d} \right)^{-3/2}. \tag{14}$$

The constants η^o, $\bar{A}$, $\bar{B}$, and $\bar{C}$ are provided by Hänel and Lehmann (1981) for each of their 10 sets of measurements. Since η^o = the limit of η as $A_w \to 1$, the $\bar{A}$, $\bar{B}$, and $\bar{C}$ terms represent the difference from the limiting value.

To evaluate the curvature part of equation (3), that is, equation (4), we must evaluate the surface tension σ, T, and r. The expression proposed by Hänel for evaluating σ is

$$\sigma = \sigma_{wo} - a(T - T_o) + b \frac{\left(\frac{m_s}{m_d} \right)}{\left(\frac{m_w}{m_d} \right)} \tag{15}$$

where $\sigma_{wo} = \sigma_w(T_o) = \sigma_w(T_o = 273.16\ K) = 75.6$ dynes/cm
$a = 0.153$ dynes $cm^{-1}\ K^{-1}$, $-10°\ C \leq T \leq 30°\ C$
b = equals a constant (different for each solute)

Hänel (verbal communication) suggests that for our application the term involving b is negligible.

To solve for r we assume that the volume of a droplet consists of the volume of the dry particulate plus the layer of water condensed onto the particle; that is,

$$v_w = \frac{4}{3}\pi\left(r^3 - r_d^{\,3} \right) \tag{16a}$$

$$v_d = \frac{4}{3}\pi r_d^{\,3} \tag{16b}$$

Taking the ratio of equations (16a) and (16b) gives

$$\frac{v_w}{v_d} = \frac{\left(r^3 - r_d^3\right)}{r_d^3} \tag{17}$$

But since $v_w = \frac{m_w}{\rho_w}$, and $v_d = \frac{m_d}{\rho_d}$, equation (17) can be expressed as

$$\frac{m_w}{m_d} = \frac{\rho_w\left(r^3 - r_d^3\right)}{\rho_d r_d^3} \tag{18}$$

or

$$\frac{m_d}{m_w} = \frac{\rho_d r_d^3}{\rho_w\left(r^3 - r_d^3\right)} \tag{19}$$

The procedure for obtaining T will be discussed in later sections of this report.

4.2 The Vertical Gradient Expression of the Equilibrium Droplet Relative Humidity

Of necessity for later developments in this report we subscript f with an r in the equations of section 4.1. In effect, if a droplet is in equilibrium with its immediate environment we designate the relative humidity as f_r. Since f_r was shown to be a function of T and r, for given r_d, we can write the differential of f_r as

$$df_r = \frac{\partial f_r}{\partial r}\, dr + \frac{\partial f_r}{\partial T}\, dT \tag{20}$$

If we then assume that f_r, r and T vary with height z, both sides of equation (20) can be multiplied by $\frac{1}{f_r}$ and divided by dz giving

$$\frac{1}{f_r}\frac{df_r}{dz} = \frac{\partial(\ln f_r)}{\partial r}\,\frac{dr}{dz} + \frac{\partial(\ln f_r)}{\partial T}\,\frac{dT}{dz} \tag{21}$$

For convenience, we write

$$\frac{\partial \ln f_r}{\partial r} = G \text{ and } \frac{-\partial \ln f_r}{\partial T} = H.$$

4.3 Nonequilibrium Model (Rachele and Kilmer)

We consider two general properties affecting all droplets: the change in mixing ratio and thermodynamics of the cluster environment as it ascends. The following symbols are used in this section:

α_e = entrainment parameter
R = radius of sphere
W_v = grams of water vapor per gram of dry air in sphere
W_v' = grams of water vapor per gram of dry air in ambient air
z = height above ground level
b = an adjustable parameter
c = an adjustable parameter
ε = ratio of molecular weight (MW) of water to mean MW of dry air = 0.621972

T' = temperature of the ambient air in kelvins
T = sphere temperature in kelvins
W_L = mass loading (liquid water plus dry material) mixing ratio inside the sphere
z_T = height above ground at top of cloud
L_e = specific enthalpy of vaporization of water at temperature of sphere
a = temperature radiation constant
C_p = specific heat of dry air at constant pressure
C_{pG} = specific heat of water vapor at constant pressure
S_L = specific heat of liquid water
S_{si} = specific heat of solid or dissolved substance i
W_{si} = grams of solid or dissolved substance i per gram of dry air

The first of two basic equations used in this development (discussed in Pruppacher and Klett (1978) for saturated conditions) describes, in differential form, the thermodynamics of an ascending "parcel." This equation has been modified in the present work and extended to our concept of a rising cluster (see section 4.4) to become

$$\frac{L_e}{C_p^*}\frac{dW_v}{dz} + \frac{dT}{dz} = -\frac{gT(1+W_v')}{C_p^* T'}\left\{\frac{1+W_v/\varepsilon}{1+W_v'/\varepsilon}\right\} + S + E + E_T + A_c + (\text{Turb}) \tag{22a}$$

where E is the "horizontal" entrainment,

$$E = -\left[\frac{L_e(W_v - W_v')}{C_p^*} + \frac{C_p^{*'}}{C_p^*}(T - T')\right]\left[\frac{3\alpha_e T}{4RT'}\right]\left[\frac{1+W_v/\varepsilon}{1+W_v'/\varepsilon}\right] \tag{22b}$$

The entrainment parameter α_e is discussed in section 4.4.

S is shedding: This effect may be considered analogous to "horizontal" entrainment represented by equation (22b) (but with mass flow in the opposite direction). However, the W_V and T of the material being shed equal the average values in the sphere. Hence, since this would be analogous to having $W_V = W_V'$ and $T = T'$ in equation (22b), $S = 0$.

E_T is the "vertical" entrainment from inversion layer above the cloud top,

$$E_T = \frac{be^{-c(z_T - z)^2}}{C_p^*} \tag{22c}$$

A_c is the net radiation effect in the cloud and is an unknown function of z,

$$A_c = F(z) \tag{22d}$$

(Turb) is the turbulence effect, after Priestley (1953),

$$(\text{Turb}) = -\frac{k_2(T - T')}{w} \tag{22e}$$

E and (Turb) are not used simultaneously in equation (22a) since they represent the same effect but are viewed from different perspectives.

C_p^* is the constant pressure heat capacity of a mass that is in the cluster sphere and that includes exactly 1 g of dry air. $C_p^{*'}$ is the analogous quantity for a mass that is in the ambient environment.

$$C_p^* = C_p + C_{pG} W_v + S_L W_L + \sum_i S_{si} W_{si} \tag{22f}$$

$$C_p^{*\prime} = C_p + C_{pG} W_v' \tag{22g}$$

In simulations using the above equations, "horizontal" entrainment or the Priestley (1953) turbulence effect tends to increase the magnitude of dT/dz when dT/dz is negative, but "vertical" entrainment from a warmer layer above the cloud decreases the magnitude of dT/dz while this gradient is negative and eventually forces dT/dz to become positive. Hence, "horizontal" entrainment and turbulence tend to increase LWC, unless the amount of liquid water that must be evaporated to bring the mixing ratio of drier entrained air up to that of damp air in the sphere exceeds the amount of liquid water gained by the effect of entrainment on dT/dz; however, "vertical" entrainment from an inversion layer decreases LWC.

Different amounts of entrainment can be modeled by adjusting α_e in equation (22b). We are not aware of a theoretical value or a theoretical expression that would generate a value for α_e. For the very low stratus clouds that we have studied to date, $\alpha_e = 0.03$ appears to be a reasonable value. Our current equation for approximating E_T is given as equation (22c). Equation (22e) is linear in the difference T - T′, which in turn is modeled as being linear with $z - z_r$, the height above the reference level. It is assumed that equation (22d) can be represented by an equation of the form

$$A_c = a(z - z_r) \tag{22h}$$

Much of the justification for including the form given as the right-hand side of equation (22h) is the empirical success enjoyed in matching observed LWC profiles with profiles simulated when this term is included. Recently Klett[2] found this term to be a reasonable approximation of gross effects of radiation. As a result of the above, equation (22a), in terms of entrainment, becomes

$$\frac{L_e}{C_p^*}\frac{dW_v}{dz} + \frac{dT}{dz} = \left\{ -\frac{gT(1+W_v')}{C_p^* T'} - \left[\frac{L_e(W_v - W_v')}{C_p^*} + \frac{C_p^{*\prime}}{C_p^*}(T - T') \right] \left[\frac{3\alpha_e T}{4RT'} \right] \right\} \times \left\{ \frac{1 + W_v/\varepsilon}{1 + W_v'/\varepsilon} \right\} + \frac{be^{-c(z_T - z)^2}}{C_p^*} + a(z - z_r) \tag{22i}$$

(In this study, the $\Sigma S_{si} W_{si}$ term is set equal to zero because the contribution from this relatively small amount of matter is negligible.)

The second basic equation describes the changes in the mixing ratio of an ascending "parcel."

---

[2] Klett, James D., unpublished report.

Pruppacher and Klett (1978) express the mixing ratio (W_v) in terms of supersaturation ($S_{v,w}$), saturation vapor pressure (e_s), and partial pressure of dry air (P_d) as

$$W_v = (1 + S_{v,w})\varepsilon \frac{e_s}{P_d} \tag{23}$$

where

$$S_{v,w} = f - 1.$$

After equation (23) is differentiated, some quantities are replaced by using the Clausius-Clapeyron expression (while neglecting the volume of liquid water produced by condensation, as neglecting this volume causes only about 5 parts per million error at a temperature of 273.16 K)

$$\frac{de_s}{dz} = \frac{L_e e_s}{R_v T^2} \frac{dT}{dz} \tag{24}$$

and the hydrostatic approximation applied to the total pressure in the environment (see derivation in the appendix)

$$\frac{dP_d}{dz} = \frac{-gP_d}{R_d T'} \left(\frac{1 + W_v'}{1 + W_v'/\varepsilon} \right) - \left(\frac{P_d}{\varepsilon + W_v} \right) \frac{dW_v}{dz} \tag{25}$$

Equation (23) in differential form, in terms of $dS_{v,w}/dz$, becomes

$$\frac{dS_{v,w}}{dz} = [1 + S_{v,w}] \left[\frac{1}{W_v} - \frac{1}{(\varepsilon + W_v)} \right] \frac{dW_v}{dz} - [1 + S_{v,w}] \left[\frac{L_e dT}{R_v T^2 dz} + \frac{g}{R_d T'} \left(\frac{1 + W_v'}{1 + W_v'/\varepsilon} \right) \right] \tag{26}$$

Equation (26) represents a significant part of droplet growth as described below.

The particles in nonequilibrium grow in accordance with Maxwell's diffusion equation, which may be written as

$$\frac{dr}{dt} = \frac{D}{r}(f - f_r) \tag{27a}$$

or, as we prefer

$$\frac{dr}{dz} = \frac{D}{rw}(f - f_r) \tag{27b}$$

where w is the cluster ascent rate, and

$$D = \left\{ \frac{\rho_w R_v T}{D_v e_v} + \frac{\rho_w L_e}{KT} \left(\frac{L_e}{R_v T} - 1 \right) \right\}^{-1} \tag{27c}$$

To evaluate equation (27b), one must have estimates of f and f_r as functions of z. We approximate them by using

$$f = f_1 + \frac{df}{dz}\Delta z \tag{28a}$$

$$f_r = f_{r1} + \frac{df_r}{dz}\Delta z \tag{28b}$$

where the subscript (1) relates to a height immediately below z, that is, z - Δz.

From equation (26), we obtain

$$\frac{df}{dz} = f\left[\frac{1}{W_v(1+W_v/\varepsilon)}\frac{dW_v}{dz} - \frac{L_e}{R_vT^2}\frac{dT}{dz} - \frac{g}{R_dT'}\left(\frac{1+W_v'}{1+W_v'/\varepsilon}\right)\right] \tag{29}$$

and from equation (21), we obtain

$$\frac{df_r}{dz} = f_r\left[G\frac{dr}{dz} - H\frac{dT}{dz}\right] \tag{30}$$

Substituting equations (28) to (30) into equation (27b) gives

$$\frac{dr}{dz} = \frac{D\Delta z}{rw}\left[\frac{(f_1-f_{r1})}{\Delta z} + \frac{f}{W_v(1+W_v/\varepsilon)}\frac{dW_v}{dz} + \left(f_rH - \frac{L_ef}{R_vT^2}\right)\frac{dT}{dz} - \frac{gf}{R_dT'}\left(\frac{1+W_v'}{1+W_v'/\varepsilon}\right) - f_rG\frac{dr}{dz}\right] \tag{31}$$

Solving equation (31) for dr/dz gives

$$\frac{dr}{dz} = \Upsilon\left[\frac{(f_1-f_{r1})}{\Delta z} + \frac{f}{W_v(1+W_v/\varepsilon)}\frac{dW_v}{dz} + \left(f_rH - \frac{L_ef}{R_vT^2}\right)\frac{dT}{dz} - \frac{gf}{R_dT'}\left(\frac{1+W_v'}{1+W_v'/\varepsilon}\right)\right] \tag{32}$$

where

$$\Upsilon = \frac{\left(\frac{D\Delta z}{rw}\right)}{\left(1+\frac{D\Delta z}{rw}f_rG\right)} \tag{33}$$

Examination of equation (32) shows that dr/dz is governed by equilibrium factors for small drops since G is approximately 3000 for r = 3 x 10^{-5} cm; hence, $D\Delta zf_rG/(rw)$ is approximately 200 for Δz = 10 cm, D = 6.16 x 10^{-7}, and w = 3 cm/s. In contrast, when r is 1 x 10^{-3} cm, G is approximately 75; hence, $D\Delta zf_rG/(rw)$ is approximately 0.15. Comparison of the latter value with 1 shows that growth of the larger drops is controlled largely by the rate of diffusion of water vapor. Therefore, the larger drops are not expected to be at their equilibrium sizes.

We initiate the solution of equation (32) by assuming that all drops are in equilibrium at z = 2 m, so that $f - f_r = 0$ for all drops. Hence, at one step above the reference height (2 m + Δz), dr/dz is evaluated for $f_1 - f_{r1} = 0$ for all drops. Above the reference height, Δz is generally set equal to 10 cm.

For each drop size class, $r(z + \Delta z)$, the drop radius at height $z + \Delta z$, typically is calculated by

$$r(z + \Delta z) = r(z) + \frac{\Delta z}{2}\left(\left.\frac{dr}{dz}\right|_{r=z} + \left.\frac{dr}{dz}\right|_{r=z+\Delta z} \right) \tag{34}$$

during the final predictor-corrector iteration for a given height step. However, during rapid evaporation, there is some danger that the last term on the right side would have a sufficiently large negative value to compromise the accuracy of the calculation and even lead to numerical instability. Therefore, no drop radius is ever allowed to decrease by more than half of the difference between that drop radius (at height z) and the dry particle radius for the same size class during a single height step (Δz).

4.4 Cluster Ascent Rate

The cluster ascent rate w is approximated using formulations that consider the effects of buoyancy, mass loading, entrainment, and turbulence. The Coriolis force is not included. The general form of the cluster ascent equation is

$$\dot{w} = g\left(\frac{\rho'}{\rho} - 1\right) - E - k_1 w \tag{35}$$

where the first term on the right includes the effects of buoyancy and mass loading, the second is due to entrainment, and the third term is due to turbulence, in line with Priestley. As was done in section 4.3, we allow either entrainment or Priestley turbulence to be activated in equation (35), but not both. If entrainment is activated in equation (35), $-k_1 w$ would be omitted, and E would be calculated as $\frac{3}{4}\frac{\rho'}{\rho}\frac{\alpha_e}{R}w^2$. R is the radius of the sphere, the initial value of which is fixed at 2 m since we generally assume the reference height to be 2 m above ground. The radius of the sphere is affected only by the change of density of dry air in the sphere.

In obtaining an expression for the density ratio ρ'/ρ in equation (35), the following items are used from assumptions 8 and 17 in section 3: It is assumed that the total air pressure of the cluster environment is equal to the total pressure of the ambient air. It also is assumed that the ambient air contains no liquid water or solid matter.

Since hydrostatic equilibrium is assumed to hold for the total pressure and density of ambient air, the ratio of the density ρ' of ambient air to the mean density ρ of the cluster environment is given by

$$\frac{\rho'}{\rho} = \frac{T(1 + W_v/\varepsilon)\left(1 + W_v'\right)}{T'(1 + W_v + W_c)\left(1 + W_v'/\varepsilon\right)} \tag{36}$$

Our formulation of entrainment (which is represented by the E term in equation (35)) considers the entrainment of ambient air into the rising cluster only; it does not account for entrainment of dry stable air above the cloud into the cloud. (However, the latter effect is represented by the last term in the cluster lapse rate equation.) The formulation evolves as follows: A rising cluster (including intimately associated damp air) displaces ambient air. The displaced air from above the cluster fills the void below, except that a small fraction α_e of the displaced mass is "entrained" into the cluster. The volume of

displaced air is equal to $\pi R^2 dz$, where R = radius of the hypothetical sphere that defines the cluster environment and dz is an infinitesimal increment of height. Therefore, the volume of air entrained while the cluster ascends by this height increment dz is $\alpha_e \pi R^2 dz$. Multiplying this volume by ρ', the density of damp air in the environment, and dividing by the mass of the cluster (including intimately associated damp air) $4\pi R^3 \rho/3$ shows that

$$\frac{1}{m}\frac{dm}{dz} = \frac{3}{4}\frac{\alpha_e}{R}\frac{\rho'}{\rho} \tag{37}$$

The work required to accelerate a given amount of mass M_1 from a velocity of (u,v,0) to (u,v,w) is taken to be equal to $M_1 w^2/2$, the gain in kinetic energy. If the change in height required for this increase in velocity is h, and the force required for this acceleration is assumed to be constant, then the force is $M_1 w^2/(2h)$. However, the total mass entrained during this change in height is h(dm/dz). Substituting this expression for M_1 shows that the total force is $(w^2/2)dm/dz$. Dividing by the total mass of the cluster and then substituting for (1/m)dm/dz shows that the force necessary to accelerate the mass being entrained per unit of total mass in the cluster is

$$E = \frac{1}{m}\frac{dm}{dz}\frac{w^2}{2} = \frac{3\,\alpha_e\,\rho'}{8\,R\,\rho}\,w^2 \tag{38}$$

This is included as part of the E term in equation (35). One of the equations used in solving for vertical gradients of temperature and water vapor mixing ratio in the cluster is obtained by extending a first law of thermodynamics equation from Pruppacher and Klett (1980) to include unsaturated conditions and condensed matter in the cluster and our approximation of a turbulence effect. When the entrainment expression from the present work is included, the resulting equation is

$$\frac{L_e}{C_p^*}\frac{dW_v}{dz} + \frac{dT}{dz} = \left\{ -\frac{gT(1+W_v')}{C_p^* T'} - \left[\frac{L_e(W_v - W_v')}{C_p^*} + \frac{C_p^{**}}{C_p^*}(T - T') \right] \left[\frac{3\pi_e T}{4RT'} \right] \right\} \times \left\{ \frac{1 + W_v/\varepsilon}{1 + W_v'/\varepsilon} \right\} + \frac{be^{-c(z_T - z)^2}}{C_p^*} + a(z - z_r) \tag{39}$$

4.5 Temperature and Potential Temperature

The temperature of the cluster environment varies in accordance with the differential form given by equation (39). Note that it is also a function of the mixing ratio of the cluster environment and the entrainment of ambient air. Based on our experience and many trials, we assume that the ambient temperature for a mature cloud phase relates to the cluster temperature as follows

$$T - T' = T_r - T_r' - \left(\frac{z - z_r}{z_T - z_r} \right)(T_r - T_r') \tag{40}$$

This equation states that the temperature difference between the cluster and ambient environments varies linearly with height, and equals zero at the top of the cloud.

The potential temperature of the cluster is stated in the traditional form as presented in R. R. Rogers (1979, 1989); that is,

$$\frac{d\theta}{dz} = \frac{\theta}{T}\left\{ -\frac{L_e}{C_p^*}\frac{dW_v}{dz} - \left[\frac{L_e}{C_p^{*\prime}}\left(W_v - W_v'\right) + \left(T - T'\right)\right]\frac{1}{m}\frac{dm}{dz}\right\} \tag{41}$$

The potential temperature of the ambient environment is based on the expression of the potential temperature of damp air; that is,

$$\theta' = T'\left(\frac{P_o}{P}\right)^{R_m/C_{pm}} \tag{42}$$

where $R_m = R_d(1 + 0.61q')$
$C_{pm} = C_{pd}(1 + 0.84q')$
P_o = 1000 millibars or 1×10^6 dynes cm^{-2}

In differential form equation (42) may be approximated by

$$\frac{T'}{\theta'}\frac{d\theta'}{dz} = \frac{dT'}{dz} + \frac{g}{C_{pm}} + T' \ln\left(\frac{P_o}{P}\right)\left(\frac{0.61R_d}{C_{pm}} - \frac{0.84C_{pd}R_m}{C_{pm}^2}\right)\frac{dq'}{dz} \tag{43}$$

4.6 Bulk Phase Change Relationship

For inclusion in a matrix equation that is appropriate at the reference height only, the phase change of moisture from vapor to liquid water is based on the change of mixing ratio of the cluster air assuming that total moisture is conserved; that is, $dW_L = -dW_V$. (This simple equality is not appropriate when entrainment and shedding are included.) To maintain consistency with other equations, we use an approximate form of equation (26) expressed in terms of f; that is,

$$\frac{1}{f}\frac{df}{dz} = \frac{1}{W_v}\frac{dW_v}{dz} - \frac{L_e}{R_v T^2}\frac{dT}{dz} - \frac{g}{R_d T} \tag{44}$$

Above the reference height, f is calculated directly as

$$f = \frac{W_v P_d}{\varepsilon e_s} \tag{45}$$

where e_s is calculated as a function of temperature according to Lowe and Ficke (1974).

4.7 Mass (Moisture) Conservation (Kilmer and Rachele)

The following assumptions are made:

a. The volume of the sphere defined by the cluster equals the total mass in the cluster sphere divided by the overall density of the cluster sphere.

b. The number of particles (droplets) N_i per cubic centimeter is inversely proportional to the volume of the cluster sphere.

c. This mass balance equation for total water must be satisfied: The sum of (1) the mass of water vapor in the sphere at height z plus (2) the mass of liquid water in the sphere at height z plus (3) the mass of water vapor gained by entrainment during height step

dz must equal the sum of (4) the mass of water vapor in the sphere at height z + dz plus (5) the mass of liquid water in the sphere at height z + dz.

d. The rate of change with height of total water mixing ratio in the sphere is equal to the rate of change of the vapor mixing ratio plus rate of change of mixing ratio of liquid water; that is,

$$\frac{dl}{dz} = \frac{dW_v}{dz} + \frac{dW_L}{dz} .$$

To help in expressing these assumptions in the form of an equation, a variable χ is defined as

$$\chi = R\left(\frac{\rho_a}{\rho_{ar}}\right)^{1/3} \tag{46}$$

The total mass of dry air in the sphere is

$$m_a = \frac{4}{3}\,\pi R^3 \rho_a \tag{47}$$

Solving equation (46) for R and substituting into equation (47) gives

$$m_a = \frac{4}{3}\,\pi \chi^3 \rho_{ar} \tag{48}$$

Taking the natural logarithm of both sides and then taking derivatives with respect to z yields

$$\frac{1}{m_a}\frac{dm_a}{dz} = \frac{3}{\chi}\frac{d\chi}{dz} \tag{49}$$

This equation shows (by multiplying both sides by χ^3) that $3\chi^2 \frac{d\chi}{dz}$ may be replaced with $\frac{\chi^3}{m_a}\frac{dm_a}{dz}$.

Using the definition of χ, assumption 3 is represented by the following equation:

$$\begin{aligned} &\frac{4}{3}\,\pi \chi^3 \rho_{ar} W_v + \left(\frac{4}{3}\,\pi\right)^2 \rho_w R_r^3 \sum_{i=1}^{N_{sc}} N_{ir}\left(r_i^3 - r_{di}^3\right) + 4\pi \chi^2 \rho_{ar} W_v' d\chi = \\ &\frac{4}{3}\,\pi (\chi + d\chi)^3 \rho_{ar} (W_v + dW_v) + \left(\frac{4}{3}\,\pi\right)^2 \rho_w R_r^3 \sum_{i=1}^{N_{sc}} N_{ir}\left[(r_i + dr_i)^3 - r_{di}^3\right] - \frac{4}{3}\,\pi R^3 \rho_a dl \end{aligned} \tag{50}$$

Starting with this equation and then

a. dividing through by $\frac{4}{3}\,\pi\, dz$, discarding the second and third powers of differentials, and collecting terms,

b. replacing $3\chi^2 \frac{d\chi}{dz}$ with $\frac{\chi^3}{m_a}\frac{dm_a}{dz}$,

c. replacing χ^3 with $\frac{R^3\rho_a}{\rho_{ar}}$,

d. replacing $\frac{1}{m_a}\frac{dm_a}{dz}$ with $\frac{3\alpha_e\rho_a'}{4R\rho_a}$,

and

e. multiplying through by $\frac{4}{3}\pi$ and rearranging the resulting equation (to facilitate identifying individual terms with physical quantities) produces

$$-\frac{4}{3}\pi R^3\rho_a\frac{dW_v}{dz} = \pi R^2\alpha_e\rho_a'(W_v - W_v') + \frac{(4\pi)^2}{3}R_r^3\rho_w\sum_{i=1}^{N_{sc}}N_{ir}r_i^2\frac{dr_i}{dz} \quad (51)$$

This equation may be interpreted as: The mass of water made available by decrease in water vapor mixing ratio with height in the sphere equals the sum of masses of water used to increase the water vapor mixing ratio of entrained air to that in the sphere and to increase the amount of liquid water in the sphere.

Multiplying both sides of this equation by $\frac{-3}{4\pi R^3}$ and rearranging again produces

$$4\pi\left(\frac{R_r}{R}\right)^3\rho_w\sum_{i=1}^{N_{sc}}N_{ir}r_i^2\frac{dr_i}{dz} + \rho_a\frac{dW_v}{dz} = -\frac{3\alpha_e}{4R}\rho_a'(W_v - W_v') \quad (52)$$

The mass balance equation in this form is represented by the next-to-last row of the matrix equation that is solved at each height level.

4.8 Drop Size Distribution

We assume that the drop size distribution at the reference height (2 m) is adequately defined by the Shettle-Fenn (1979) formulation as discussed in this section.

Shettle and Fenn use a bimodal lognormal distribution

$$n(r) = \frac{dN(r)}{dr} = \sum_{i=1}^{2}\left[\frac{N_i}{r\,\sigma_i(2\pi)^{1/2}\,\ln(10)}\right]\exp\left[-\frac{(\log r - \log r_i)^2}{2\sigma_i^2}\right] \quad (53)$$

where

$N(r)$ = the cumulative number density of particles of radius r
σ_i = the standard deviation
r_i = the mode radius
N_i = the number density corresponding with r_i

Four different aerosol models for the atmospheric boundary layer near the earth's surface were developed by Shettle and Fenn. The models differ in particle size distribution and

particle refractive index. Table 1 lists the parameters defining the size distributions in accordance with equation (53) for these models.

The choices of N in table 1 were normalized by Shettle and Fenn to correspond to 1 particle/cm^3. The actual size distributions can be renormalized for the visibility being used, or one can use a distribution from those characterized by tables 3, 4, and 5 for rural, urban, and maritime conditions, respectively.

TABLE 1. CHARACTERISTICS OF THE AEROSOL MODELS OF THE LOWER ATMOSPHERE (SHETTLE AND FENN, 1979)

Aerosol Model	Size Distribution			Type
	N_i	r_i*	σ_i	
RURAL	0.999875 0.000125	0.03 0.5	0.35 0.4	Mixture of water-soluble and dust-like aerosols
URBAN	0.999875 0.000125	0.03 0.5	0.35 0.4	Rural aerosol mixture with soot-like aerosols
MARITIME				
Continental Origin	1.	0.03	0.35	Rural aerosol mixture
Oceanic Origin	1.	0.3	0.4	Sea salt solution in water
TROPOSPHERIC	1.	0.03	0.35	Rural aerosol mixture

* These mode radii correspond to moderate humidities (70 to 80 percent); values of r_i as function of humidity are given in table 2.

TABLE 2. MODE RADII FOR THE AEROSOL MODELS AS A FUNCTION OF RELATIVE HUMIDITY (SHETTLE AND FENN, 1979)

Relative Humidity (%)	Tropospheric	Rural		Maritime	Urban	
	r_1	r_1	r_2	r_2	r_1	r_2
0	0.02700	0.02700	0.4300	0.1600	0.02500	0.4000
50	0.02748	0.02748	0.4377	0.1711	0.02563	0.4113
70	0.02846	0.02846	0.4571	0.2041	0.02911	0.4777
80	0.03274	0.03274	0.5477	0.3180	0.03514	0.5805
90	0.03884	0.03884	0.6462	0.3803	0.04187	0.7061
95	0.04238	0.04238	0.7078	0.4606	0.04904	0.8634
98	0.04751	0.04751	0.9728	0.6024	0.05996	1.1691
99	0.05215	0.05215	1.1755	0.7505	0.06847	1.4858

The radii in the above table are in micrometer (μm) units.

TABLE 3. TOTAL NUMBER DENSITY FOR THE RURAL AEROSOL MODEL AS A FUNCTION OF RELATIVE HUMIDITY AND METEOROLOGICAL RANGE (SHETTLE AND FENN, 1979)

Relative Humidity =	0%	50%	70%	80%	90%	95%	98%	99%
Visibility = 2 km								
N1 =	199530.58	192537.16	178656.10	129883.79	85526.28	68260.42	48674.99	37244.91
N2 =	24.94	24.07	22.33	16.24	10.69	8.53	6.09	4.66
Visibility = 5 km								
N1 =	79076.33	76304.75	70803.53	51474.48	33895.07	27052.41	19290.47	14760.60
N2 =	9.89	9.54	8.85	6.44	4.24	3.38	2.41	1.85
Visibility = 10 km								
N1 =	38924.91	37560.62	34852.67	25338.05	16684.67	13316.41	9495.64	7265.83
N2 =	4.87	4.70	4.36	3.17	2.09	1.66	1.19	0.91
Visibility = 23 km								
N1 =	16230.63	15661.76	14532.62	10565.23	6957.06	5552.58	3959.42	3029.65
N2 =	2.03	1.96	1.82	1.32	0.87	0.69	0.49	0.38
Visibility = 50 km								
N1 =	6803.78	6565.31	6091.98	4428.90	2916.35	2327.61	1659.76	1276.01
N2 =	0.85	0.82	0.76	0.55	0.36	0.29	0.21	0.16

TABLE 4. TOTAL NUMBER DENSITY FOR THE URBAN AEROSOL MODEL AS A FUNCTION OF RELATIVE HUMIDITY AND METEOROLOGICAL RANGE (SHETTLE AND FENN, 1979)

Relative Humidity =	0%	50%	70%	80%	90%	95%	98%	99%
Visibility = 2 km								
N1 =	220039.51	210325.47	163580.19	107935.91	69877.38	45967.45	26535.53	18383.38
N2 =	27.51	26.29	20.45	13.49	8.74	5.75	3.32	2.30
Visibility = 5 km								
N1 =	87204.26	83354.47	64828.76	42776.28	27693.23	18217.44	10516.34	7285.35
N2 =	10.90	10.42	8.10	5.35	3.46	2.28	1.31	0.91
Visibility = 10 km								
N1 =	42925.84	41030.80	31911.62	21056.40	13631.85	8967.44	5176.62	3586.27
N2 =	5.37	5.13	3.99	2.63	1.70	1.12	0.65	0.45
Visibility = 23 km								
N1 =	17898.91	17108.73	13306.28	8779.95	5684.11	3739.18	2158.51	1495.38
N2 =	2.24	2.14	1.66	1.10	0.71	0.47	0.27	0.19
Visibility = 50 km								
N1 =	7503.11	7171.87	5577.91	3680.50	2382.74	1567.44	904.83	626.85
N2 =	0.94	0.90	0.70	0.46	0.30	0.20	0.11	0.08

TABLE 5. TOTAL NUMBER DENSITY FOR THE MARITIME AEROSOL MODEL AS A FUNCTION OF RELATIVE HUMIDITY AND METEOROLOGICAL RANGE (SHETTLE AND FENN, 1979)

Relative Humidity =	0%	50%	70%	80%	90%	95%	98%	99%
Visibility = 2 km								
N1 =	96516.79	88640.83	70038.09	35078.01	24467.13	17603.12	11000.60	7438.74
N2 =	974.92	895.36	707.46	354.32	247.14	177.81	111.12	75.14
Visibility = 5 km								
N1 =	38250.75	35129.41	27756.92	13901.83	9696.61	6976.32	4359.67	2946.06
N2 =	386.37	354.84	280.37	140.42	97.95	70.47	44.04	29.78
Visibility = 10 km								
N1 =	18828.73	17292.27	13663.20	6843.10	4773.11	3434.06	2146.02	1451.17
N2 =	190.19	174.67	138.01	69.12	48.21	34.69	21.68	14.66
Visibility = 23 km								
N1 =	7851.07	7210.41	5697.18	2853.39	1990.26	1431.91	894.83	605.10
N2 =	79.30	72.83	57.55	28.82	20.10	14.46	9.04	6.11
Visibility = 50 km								
N1 =	3291.12	3022.56	2388.22	1196.12	834.30	600.25	375.11	253.65
N2 =	33.24	30.53	24.12	12.08	8.43	6.06	3.79	2.56

The Shettle-Fenn distribution has three constraints; that is, the distribution depends on visibility, relative humidity, and aerosol origin (maritime, urban, or rural).

The selected distribution is used to determine the number of droplets in each size class as defined at the reference level. Lower and upper bounds, r_a and r_b, respectively, are set for the droplet radius in each size class. The number of droplets in a given size class is

$$\int_{r_a}^{r_b} n(r)dr,$$

where n(r) is defined in equation (53) at the reference level. Above the reference level, the number of droplets per cubic centimeter in a given size class is inversely proportional to the volume of the sphere. At the reference level, the representative radius for that size class is calculated as the mean volume radius for $r_a \leq r \leq r_b$; that is,

$$\left[\int_{r_a}^{r_b} r^3\, n(r)\, dr \Big/ \int_{r_a}^{r_b} n(r)\, dr\right]^{1/3}$$

This form was chosen because of the importance of r^3 in calculating mass loading. The representative radius is used with the relative humidity at the reference level to solve the modified Hänel droplet growth equation iteratively for the radius of the dry particles of this size class. Once determined, the radius of dry particles for each size class remains constant throughout the modeling. However, the representative droplet radius for each size class of evolving droplets is allowed to change without regarding r_a and r_b.

4.9 Solution Matrix

The system of equations that defines the model is written and solved in matrix form. At the reference height, the equations consist of the equilibrium particle growth formulation (which can be obtained by substituting equations (5), (12), and (13) into equation (7) and differentiating); equation (44), the bulk phase change relationship; equation (52), the moisture conservation equation including the drop size distribution; and equation (22a), the thermodynamics of the ascending sphere. Above the reference height, the equations consist of equation (32), the nonequilibrium growth expression; equation (52); and equation (22a).

To obtain reasonable accuracy in reasonable computation time, we generally divide the drop size distribution into 80 size classes; therefore, the basic set of equations consists of 82 equations (83 at the reference height). For high accuracy, 1000 size classes are sometimes used. For purposes of illustration, a matrix equation for use above the reference height is shown below for a compressed set of equations consisting of only one size class.

$$\begin{bmatrix} 1 & A & B \\ 4\pi\left(\frac{R_r}{R}\right)^3 \rho_w N_{1r} r_1^2 & \rho_a & 0 \\ 0 & \frac{L_e}{C_p^*} & 1 \end{bmatrix} \begin{bmatrix} dr_1/dz \\ dW_v/dz \\ dT/dz \end{bmatrix} = \begin{bmatrix} C \\ Y_{N_{sc}+1} \\ Y_{N_{sc}+2} \end{bmatrix} \tag{54}$$

$$A = -\Upsilon \frac{f}{W_v(1 + W_v/\varepsilon)} \tag{55a}$$

$$B = -\Upsilon\left(f_r H - \frac{L_e f}{R_v T^2}\right) \tag{55b}$$

$$C = \Upsilon\left[\frac{(f_1 - f_{r1})}{\Delta z} - \frac{gf}{R_d T'}\left(\frac{1 + W_v'}{1 + W_v'/\varepsilon}\right)\right] \tag{55c}$$

$$D = \left[\frac{\rho_w R_v T}{D_v e_v} + \frac{\rho_w L_e}{KT}\left(\frac{L_e}{R_v T} - 1\right)\right]^{-1} \tag{55d}$$

$$\Upsilon = \frac{\left(\frac{D\Delta z}{rw}\right)}{\left(1 + \frac{D\Delta z f_r G}{rw}\right)} \tag{55e}$$

$$f_r = \exp\left[\frac{2v_w\sigma}{R_v T r} - \frac{\eta\rho_d}{\rho_w}\left\{\left(\frac{r}{r_d}\right)^3 - 1\right\}^{-1}\right] \tag{55f}$$

$$\eta = \eta^0\left[1 + \sum_{j=1}^{6} a_j\left(\frac{r_d}{r}\right)^j\right] \tag{55g}$$

$$Y_{N_{sc}+1} = -\frac{3\alpha_e}{4R}\rho_a'(W_v - W_v') \tag{55h}$$

$$Y_{N_{sc}+2} = \left\{-\frac{gT(1 + W_v')}{C_p^{\cdot} T'} - \left[\frac{L_e(W_v - W_v')}{C_p^{\cdot}} + \frac{C_p^{\cdot\cdot}}{C_p^{\cdot}}(T - T')\right]\left[\frac{3\alpha_e T}{4RT'}\right]\right\} \times \left\{\frac{1 + W_v/\varepsilon}{1 + W_v'/\varepsilon}\right\} + \frac{be^{-c(z_T - z)^2}}{C_p^{\cdot}} + a(z - z_r) \tag{55i}$$

G, H, r_d, and η depend on the droplet size and thus may be subscripted to indicate the droplet size class. At the reference height, all droplets are assumed to be in equilibrium with the air. At each level above the reference height, the growth of droplets is limited by rates of diffusion of water vapor and heat transfer to and from droplet surfaces.

A, B, and C in equations (55a), (55b), and (55c) are derived in a way that assures that droplet growth does not exceed the rate allowed by diffusion. G and H in equations (55e) and (55b) are values (as defined just after equation (21)) originating from the modified Hänel droplet growth model (1981) for drops that are in equilibrium with the atmosphere.

5. MODEL EVALUATION

It is apparent in analyzing our model equations that the vertical profiles of the drop size distribution and associated parameters can vary considerably, but we feel in a sensible way. For instance, Shettle and Fenn (1979) require that their drop size distributions, which we use to define drop size distributions for our model at the reference height, vary significantly as a function of relative humidity, visibility, and geography. However, we truncate these distributions to remove the smallest drops (those that would have condensation nuclei with equivalent dry sphere radii less than 0.04 μm) because of scavenging effects (Huser and Holloway, 1984; Hänel, 1984). Another source of variability is reported by Hänel and Lehmann (1981), who show that the equilibrium sizes of drops are sensitive to the temperature and relative humidity of their immediate environment (which would be inside the sphere in the present study) and the chemistry of the dry nuclei, which also vary with geography; especially significant is the contrast between those continental and maritime nuclei that belong to the larger-radius modes of bimodal distributions. We, in turn, have shown that drops in a nonequilibrium state with their immediate environment grow quite differently than do those assumed to be in an equilibrium state. Unfortunately, some results in the literature are based on the assumption that drops are in equilibrium with their environment, which tends to exaggerate the size of the larger droplets.

Our model also shows that the growth rates of the drops vary according to the ascent rate of the sphere, and that the ascent rate of the sphere varies with buoyancy, mass loading, entrainment, and the initial ascent rate of the sphere. In turn, the buoyancy varies with the temperature and composition of the environment; the mass loading varies with a number of factors, including stability and thermodynamics. Finally, the bulk thermodynamics is a function of temperature, pressure, and relative humidity. Many factors interact in a very complicated way. With all the assumptions and interactions that go in the model, it is gratifying to obtain drop size distributions that make any sense at all. On the other hand, it should be no surprise at all that drop size distributions vary as much as reported in the literature.

When we started to evaluate our model, we were surprised to find that no (so few) measurements are available of the type and resolution required. The largest known sets of data are those that were collected in Germany, mentioned in the Introduction, and they are seriously limited for several reasons, the most critical being that reliable temperature, relative humidity, and wind profiles were not obtained while collecting the drop size and concentration data. Furthermore, according to Lala et al. (1987) and Loveland and Lindberg (1988), the drop data are highly suspect in the very low and high LWC ranges. Nevertheless, we examined several cases of measured data from Meppen with emphasis on vertical profiles of liquid water content and drop size distributions.

We viewed the very low stratus clouds as if they have characteristics lying between fog and higher stratiform clouds and, in some cases, even low cumulus, for which there are a number of reported cases in the literature. Our comparisons are both qualitative and quantitative where possible. We chose the following parameters for comparison: temperature, relative humidity, liquid water content, and drop size distribution.

The comparisons that follow are based on sets of realistic conditions that we specified to initialize our model. For all three modeled examples used here, Shettle-Fenn distribution parameters for a maritime air mass were used, the initial value for the ascent rate of the

cluster sphere was 3 cm/s, and the sphere radius at the reference (initial) height was 2 m (which is the same value as the reference height above ground level). Other values used as input to the model are listed in table 6.

TABLE 6. INPUT FOR RK MICROPHYSICS MODEL

Corresponding Meppen 80 profile no. -->	5	6	7
Lower cutoff (μm) *	0.04	0.04	0.04
Entrainment parameter α_e	0.03	0.03	0.03
a in cluster lapse rate equation	1.4×10^{-9}	2×10^{-9}	1.4×10^{-9}
b in cluster lapse rate equation	8×10^{3}	6×10^{3}	1×10^{4}
c in cluster lapse rate equation	2×10^{-7}	8×10^{-8}	1.5×10^{-6}
Initial height (m)	2.00	2.00	2.00
Height of top of cloud (m)	280	320	290
Input values at initial height:			
Visibility (km)	1.9	1.4	1.02
Relative humidity in cluster	0.93	0.944	0.96
Pressure (millibars) **	1016	1015	1015
Temperature in cluster (K)	272.33	272.36	272.54
Temperature of ambient environment (K)	272.25	272.26	272.24

* Lower cutoff is the smallest dry particle (condensation nucleus) radius (μm) allowed.
** Pressure at initial height is the total pressure (in millibars) due to air and water vapor.

5.1 Temperature and Relative Humidity

A common approach for computing the vertical temperature profile below a cloud (especially cumulus) is to assume that from the surface to the base of the cloud conditions are dry adiabatic, and in the cloud conditions are moist adiabatic. Our model shows that the cluster lapse rate is close to dry adiabatic or superadiabatic at reference level and decreases to approximately moist adiabatic near the base of the cloud. In the lower part of the cloud where relative humidity is maximum, the lapse rate of the cluster is a little greater than the moist adiabatic value. This effect and the superadiabatic lapse rate at reference level both appear to be consequences of cooler, drier air being entrained into the cluster. At the same time, our model shows that the ambient environment lapse rate may vary from slightly greater than dry adiabatic to between dry adiabatic and moist adiabatic in the subcloud region. The cluster and ambient atmosphere (environmental) lapse rates are shown in figure 5, and the temperature profiles in figure 6 for the three cases that we considered in this study. Note from figure 6 that it would be difficult to measure the differences between cluster and ambient temperatures, which are never greater than 0.3 K for these examples. Noonkester (1982) presents measured temperature and relative humidity profiles for several maritime stratus clouds. We chose one case from his figure 2 for illustrative purposes, figure 7. Note that the vertical structure of both the temperature and relative humidity curves is generally in line with our model results. Also, note that Noonkester's data were collected during warmer conditions, so

that the moist adiabatic lapse rate is smaller than some of our cases when the temperature was near zero degrees centigrade. For stratocumulus clouds, Kao and Yamada (1989), Nicholls (1984), and Slingo et al. (1982b) found that the temperature gradient is approximately dry adiabatic in the subcloud region and near moist adiabatic in the cloud. For stratocumulus and stratus clouds, Borovikov (1963) concluded that under the clouds the lapse rate remained lower than the dry adiabatic lapse rate all year. Whereas, in the cloud there are two kinds: either a more or less uniform lapse rate approaching the moist adiabatic lapse rate, or a thin inversion layer is present in the upper region of the cloud layer and the cloud "wedges" into the overlying main inversion. From the above results we concluded that the temperature profiles provided by our model are well in line with what should be expected.

In addition to the temperature profiles we also computed the potential temperature gradient profiles of the cluster and ambient atmosphere for the cases presented in figures 5 and 6. Results are shown in figure 8. Note that the potential temperature gradient of the cluster is negative from the surface to approximately 77, 73, and 167 m above ground level for profiles 5, 6, and 7, respectively, and then becomes positive, suggesting unstable conditions in the lower part of the profile and stable conditions above these heights. In the ambient environment, the corresponding gradients are negative from the surface up to about 34, 32, and 64 m above ground level and positive above these heights, suggesting stable conditions start at lower levels in the ambient environment.

5.2 Liquid Water Content

We use the term mass loading to include both liquid water and dry particle (nuclei) material. Field measurements are actually mass loading values. In our model we can separate the contributions of each; however, the field measurements do not lend themselves to this treatment. There are usually no serious violations if one assumes that the drops are all water in the truncated distribution used in our model. However, caution must be used, for example, when modeling absorption for wavelengths at which the imaginary part of the index of refraction is much larger for the nuclear material than for pure water.

Estimates of liquid water content in clouds are most controversial. For us they are most frustrating. One can defend within reason any estimate of LWC in clouds that one chooses based on results published in the literature. The situation is even worse in the subcloud region. Warner (1970), who is quoted quite frequently in the literature (for instance Pruppacher and Klett, 1978; Rogers et al., 1985); references studies by Ackerman (1959, 1963), Skatski (1965), and Warner and Squires (1958) from which he states that the ratio of measured to adiabatic liquid water decreases with height above cloud base. In contrast, Driedonks and Duynkerke (1989), referencing Slingo et al. (1982 a,b) and Nicholls (1984) concludes that for stratocumulus clouds the mean liquid water content distribution is very close to the adiabatic value, and according to Nicholls (1984) earlier measurements of liquid water content that gave values much smaller than the adiabatic ones are not reliable due to instrumental inaccuracies. However, according to Slingo et al. (1982b), who studied nocturnal stratocumulus, the liquid water path from a microwave radiometer on the average gave values 0.7 times the value for adiabatic ascent. Rogers et al. (1985) state that for stratiform clouds (St, Ns and As) the adiabatically generated LWC is used at its full value since entrainment is relatively unimportant in wide spread layered clouds. At the other end of the spectrum are conclusions by Mao Jie-tai et al. (date unknown), who reference Borovikov (1961), Singleton and Smith (1960) and measurements at Wang-

Jih-tai during the period September 1960 to March 1961, that the liquid water content in layer clouds exceeded adiabatic values by as much as a factor of 2.

When studying cloud condensation nuclei (CCN) and supersaturation of stratus clouds, Hudson (1983) concluded that stratus clouds can have strong adiabatic characteristics.

Liquid water content estimates from recent measurements using Knollenberg sensors are supported by some, adjusted by others, and argued to be in error by factors of 2 to 4 in the range of values in clouds and a factor of 5 in subcloud regions by Lala (1987) and Loveland and Lindberg (1988).

Low (1980) presents quite a different picture of the LWC profile in stratus clouds based on data from the Soviet Union (Khrgian, 1963) and data from Germany. For stratus clouds defined by Koening and Schutz (1974) as having bases ranging from 0.1 to 1.0 km, Low found that the LWC varies parabolically with height above the base of the cloud as

$$LWC = A(0) + A(1)z + A(2)z^2$$

where

$$A(0) = 0.1193$$

$$A(1) = 1.99 \times 10^{-3}$$

$$A(2) = -1.475 \times 10^{-6}$$

LWC is in g m^{-3} and z in meters.

The value of A(0) would be suspect by many researchers who are inclined to assume that the LWC at cloud base is zero.

In the examples calculated by our model for this report, the LWC values were subadiabatic in the subcloud region having a profile curvature consistent with cloud measurements made in Germany (see figure 1). In the cloud itself the model produced values ranging from 0.5 to 0.75 of adiabatic to agree with measured values, except near the cloud base where relative humidity is a maximum. See figure 9. LWC profiles reported by Noonkester (1984) for maritime stratus are similar in structure to those simulated by our model (figure 10). Our strategy was to adjust the cloud LWC values so that they would be in line with experimental results by introducing a radiation effect (see section 4.3, especially equations (22a), (22d), and (22h)). At this time it is not clear as to how much adjustment should be made in general, but a reasonable mechanism for doing so is in the model. It also allows for entrainment effects due to dry air insertion from above the cloud.

5.3 Supersaturation

Hudson (1983) concluded that the supersaturation of stratus clouds is consistent with the concept of a moderate updraft intermediate between values determined for fog and cumulus clouds. For stratus clouds with bases between 300 and 600 m, he found that the effective supersaturation is on the order of 0.17 percent which is less than the more strongly convective cumulus clouds [for example, up to 1 percent (Twomey, 1959)] but greater than that of the less active fogs [~0.10 percent (Fitzgerald, 1978; Hudson, 1980;

Meyer et al. 1980)]. More recently Hudson (1986) discusses the results of four field measurements. Two of these involved stratus clouds "impacted" on California coastal mountains, while the other two sites (1425 and 1520 m elevation) involved fogs in Reno, Nevada. The California sites were Henninger Flats (765 m elevation) near Pasadena, and San Marcos pass (660 m elevation) near Santa Barbara. Hudson found that the effective supersaturation ranged from 0.02 to 0.05 percent at Henninger Flats, and $>$ 0.1 percent at San Marcos Pass, but the Henninger Flats values were questionable due to measurement resolution problems. The maximum supersaturation produced by our model for the three cases considered in this study (see figure 11) was 0.043 percent, which is smaller than most of those suggested by Hudson. This value was obtained for simulated profile 7; the other two profiles did not reach saturation. These small maximum relative humidity values are attributed to the very hygroscopic nature of the condensation nucleus type (that of Hänel-Lehmann sample number 4) chosen for all three model examples.

5.4 Drop Size Distribution Comparison

We introduce this section with some comments about the basic features of drop size distributions as we perceive and use them. First, we choose a reference height drop size distribution as defined by Shettle and Fenn (1979) for specified values of relative humidity and visibility. We then truncate this distribution to remove the smallest drops of the distribution.

We presume that the smallest drops are removed from the distribution due to scavenging as discussed by Husar and Holloway (1984) and Hänel (1984). The dry particle size distribution was determined by using the truncated Shettle-Fenn distribution and assuming equilibrium at reference height. The damp reference height drop size distribution is shown in figure 12; the dry particle size distribution at the reference height is shown in figure 13. In effect, for the cases presented in this report, our droplets have a minimum dry radius of 0.04 μm and maximum dry radii of about 53, 49, and 45 μm for modeled profiles 5, 6, and 7, respectively.

The drops in this truncated distribution grow in accordance with our formulations, given in section 4.2, as they are lifted within the rising cluster (see figure 14). The results are generally consistent with Hudson (1983) who states that these subcloud concentrations consist mostly of enlarged haze particles that have not reached their critical size, but the relative humidity is high enough to produce detectable haze droplets. As the drops continue to rise above the height of maximum relative humidity, some drops may be small enough to start evaporating after an initial period of growth, larger drops may become activated,[3] and the largest drops are growing although still subsaturated. In a number of model results, drops in some of the smaller size classes appear to first be activated but then shrink to become haze droplets. This behavior looks strange but is consistent with the model. The model does not allow water vapor to diffuse from a region of lower relative humidity to a region of higher relative humidity, even when the latter is in equilibrium with the surface of a drop having a radius greater than the radius at critical supersaturation. The relative humidity of air in a cluster in a lower region of the cloud exceeds the critical supersaturation value for drops in these size classes. Thus, although showing some lag in growth (compared with equilibrium drop size) from diffusion limitation on

---

[3] A condensation nucleus is said to be "activated" when the droplet formed around it reaches its critical size (Rogers and Yau, 1989).

drop growth, drops in these size classes become activated. However, closer to the top of the cloud, the relative humidity of air in the cluster decreases with height and becomes less than the relative humidity at the surface of the drop. Thus, some water evaporates from the drop, even if its radius is greater than the critical supersaturation value, and the drop becomes deactivated.

The fast growth rate of many of the drops is consistent with Korolev et al. (unknown) who found that the condensation nuclei begin to take on significant water at approximately 10 to 15 m below the cloud base. However, our results are in conflict with Hudson's (1983) proposition that the largest drops are the first to become activated. As the droplets continue to rise we notice that the smaller droplets undergo some evaporation while the larger drops continue to grow. Interestingly enough, the largest drops do not achieve their critical supersaturation values up to the cloud top, but, even so, continue to be larger than those that do. Hence additional spectrum broadening is noted and the average drop size increases (figures 14 and 15). The model results are supported by several studies, for instance, Singleton et al. (1960) in studying low layer clouds found that there is a distinct trend for spectra to become broader as cloud thickness increases. In his paper of CCN measurements within clouds Hudson (1984) notes that Baker et al. (1980) proposed that inhomogeneous mixing resulted in the evolution of broadened droplet spectra. Hudson, however, found that homogeneous mixing is sufficient to explain this broadening, and our results support this view. Pruppacher and Klett (1978) also state that the drop spectrum becomes broader as the cloud thickness increases. Slingo et al. (1982b) in observing marine stratocumulus found that the mean drop radius increased steadily towards cloud top, and that there was a systematic increase of mode radius from about 5 μm at cloud base to 11 μm at cloud top. These values should vary depending on the height of the cloud base and the height of the cloud top. Korolev et al. (unknown) when observing stratiform clouds found that at the condensation level, water containing nuclei, depending upon their degree of ascent, grow rapidly, and the average droplet size increases. Similarly, Slingo et al. (1982a) observed in nocturnal stratocumulus that in two thick clouds the drop size data showed an almost monotonic increase of mean radius from cloud base to top. The mode radius increased from about 3 μm at cloud base to about 8 μm at cloud top. Nicholls (1984) in studying a stratocumulus cloud over the North Sea found an increase in the mean volume radius (r_v) of the drops as shown in figure 16. In this case the cloud base was approximately 400 m. Slingo et al. (1982b) in studying marine stratocumulus found that the mean radius varied as shown in figure 17 using data collected with an ASSP. Goodman's (1976) summary of California coastal fog and stratus shows a consistent fog microstructure with mean diameters increasing with height, drop size distributions broadening with height, and liquid water content increasing with height.

If one chooses to define the number of cloud drops as those that are activated, this number is zero until the cluster gets above the height of maximum relative humidity, which in our case is a relatively short distance above cloud base. Above the height of maximum relative humidity, the number of activated drops exhibits a few fluctuations of considerable magnitude, largely owing to the behavior of droplets in the smallest few size classes retained in the distribution. If one elects to define the number as a sum of the activated and the largest drops, the number is not much different from the number of activated drops since there are so few in the largest drop sizes. Note, however, that this count is sensitive to the behavior of the smallest size classes. In computing extinction for different wavelengths, we must also be concerned with the smaller droplets even though they are not activated. Finally, the measured drop size distribution is strongly a function

of the sensors used, especially since there are large numbers of drops in the smallest size classes.

These features are illustrated in figure 18 where we plotted the concentration of drops as a function of height, resulting from our model, for lower cutoff values of 0.25, 0.5, and 1.0 μm for the drop radius for profile 7. As a general qualitative comparison we show measured concentration profiles. For instance, in figure 19 we have a drop concentration profile of a marine stratocumulus cloud, observed by Slingo et al. (1982b) using an ASSP. The base of the cloud was approximately 500 m and the top was 900 m. Similarly, we show drop concentrations (number density) for three cases (figures 20, 21, and 22) of nocturnal stratocumulus studied by Slingo et al. (1982a). The drops were measured with an ASSP probe with a cutoff of 1 μm radius. Nicholls (1984) presents a drop concentration profile, figure 23, for stratocumulus using an ASSP (cutoff 1 μm). Figures 24 and 25 show a comparison of continental (San Diego) and maritime droplet concentrations measured by Hudson (1983) with an ASSP (cutoff 0.3 μm radius). Note that the measured data had lower drop cutoff radii as indicated, because of instrumental range; whereas the simulated data (such as shown in figure 18) had lower cutoffs of whatever wet radii corresponded to dry radii of 0.04 μm. These smallest values of wet radii vary with relative humidity, which in turn varies with height.

Knollenberg aerosol spectrometers of the type (FSSP-100C) used to acquire Meppen 80 data (see Lindberg, 1982) are known to underestimate drop concentrations when the liquid water content is low. According to Lala et al. (1987), and independently by Loveland and Lindberg (1988), the liquid water content derived from measured drop size and number data can be in error by as much as a factor of 10 when the liquid water content is low. Hence, we concluded that, for the subcloud region in cases presented in this study, the liquid water content, drop number, and mean volume radius derived from the measured data are in error, likely being worse near the ground and better near the cloud base. Furthermore, the visibility estimates would also be in error. For instance, for profile 5 the measured visibility at the lowest height was 1.9 km; whereas the visibility computed by applying Mie theory (to spheres of pure water using measured drop size and number data) and Koschmieder's relationship was 13.2 km. In contrast, based on the studies by Lala et al. (1987) and Loveland and Lindberg (1988), we concluded that the drop size and number, and consequently liquid water content and mean volume radius, estimates are reasonable in the cloud.

SUMMARY AND CONCLUSIONS

We feel that we have structured a theoretically based model that provides reasonable internally consistent "average" vertical profiles of temperature, pressure, density, potential temperature, specific humidity, relative humidity, liquid water content, and drop size distribution in very low stratus clouds and their associated subcloud regions. We also feel that combinations of these profiles can be useful to Army users, including researchers concerned with moisture effects on EO sensors, systems and electromagnetic propagation. Furthermore, we feel that we achieved the goal of designing a model that requires a minimum number of conventional surface (2 m above ground) meteorological inputs, that is, temperature, pressure, and relative humidity. However, we did find it necessary to know (specify) the height of the cloud top; type of nucleus; and the rate of ascent, radius of cluster sphere, and a visibility parameter at 2 m above ground. We certainly did not achieve the simplification of input attained in models by Duncan (1980) and Heaps (1982) who require only one surface input to compute "gross average" empirically based

liquid water content or extinction profiles. However, it is apparent from analyzing our model that because of the number of inputs required we can expect significant variation in the profiles, particularly on a worldwide scope. Lastly, we also managed to structure the model so that it can be executed on a comparatively small computer (HP9000-840).

Most of the vertical profiles produced by the model are generally in line with field observations. However, for some cases there is considerable variability in the observed liquid water content profiles. This is unfortunate, since we had decided to adjust our model so that the model liquid water content profiles would generally agree with field observations. Furthermore, there is such a large variation in the observations, and controversy by authors, that we are not sure of the best way to adjust the liquid water content profiles. We have used selected liquid water content profiles calculated from measured data to suggest desired values in the cloud region.

Our vertical profiles of drop size distribution are generally in line with the literature. We show a broadening of the distribution above the height of maximum relative humidity and an increase in the average or mode drop radius with height. It is important to note that the size distribution of drops is also changing with height.

In the subcloud region all droplets, since they are in subsaturated air, are damp haze type that grow in size monotonically from the surface to the base of the cloud. Once in the cloud, the smallest of these haze droplets tend to evaporate somewhat so that the drops decrease in size with height. In the version of the model presented in this report, these smallest droplets were among those omitted from the truncated distribution.

The following features and results of our model are different from some in the literature. Our model is a nonequilibrium model. That is to say, the smallest drops of the distribution are very close to being in equilibrium with their environment (in cluster), but all the larger ones are in nonequilibrium to some degree: Rates of drop growth are limited by the rates of diffusion of water vapor to the drop surfaces. This is especially significant since the largest drops are not allowed to grow as large as they would if they were permitted to be in equilibrium. This leads us to another point of difference. Hudson (1983) has concluded that the largest drops of the distribution are activated first. We find, in contrast, that the midsized drops are activated first. In fact, the largest drops do not become activated by the time they reach the top of the cloud in our examples. Even so, they are always larger in size than the activated drops.

Finally, we found no mathematical or physical reasons suggesting that the vertical profiles of all parameters are not continuous for clouds whose bases are less than 300 m. Hence, we feel that the unification of the cloud and subcloud region is justified as was done in the model development.

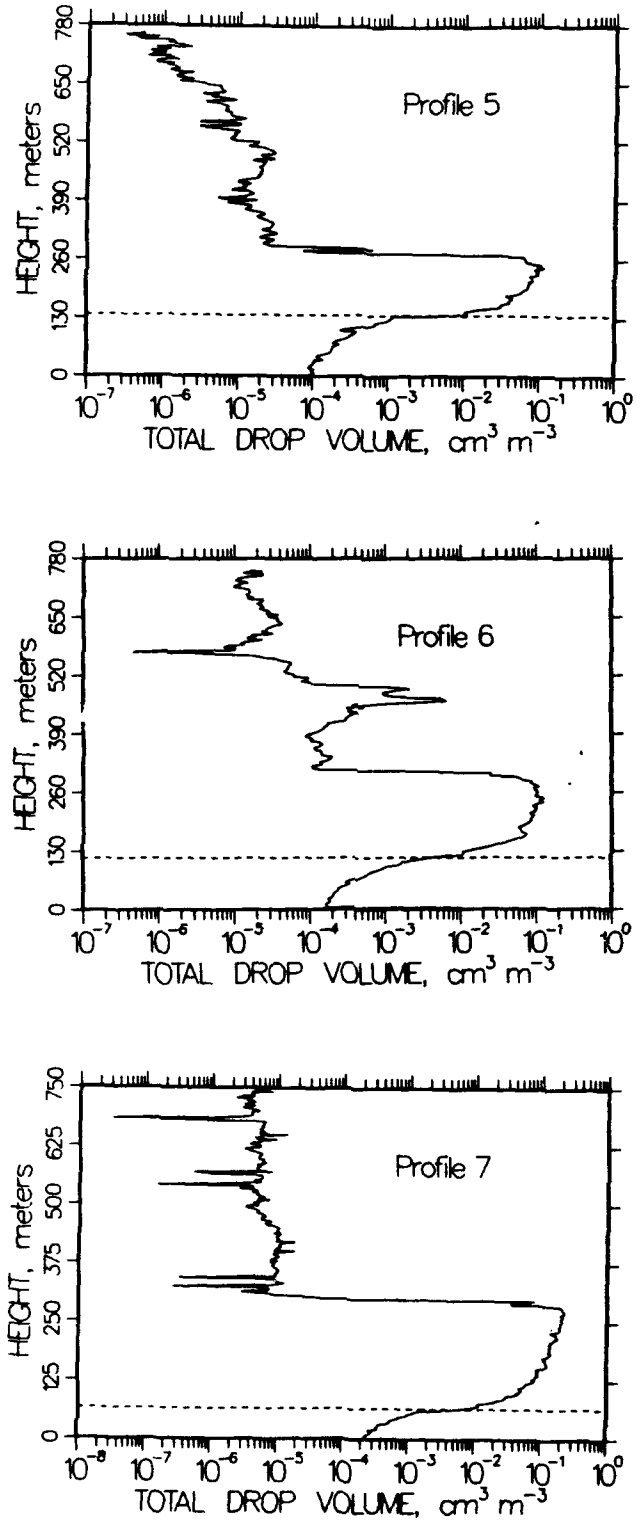

Figure 1. LWC profiles from observed data (Meppen, Germany, 1980).

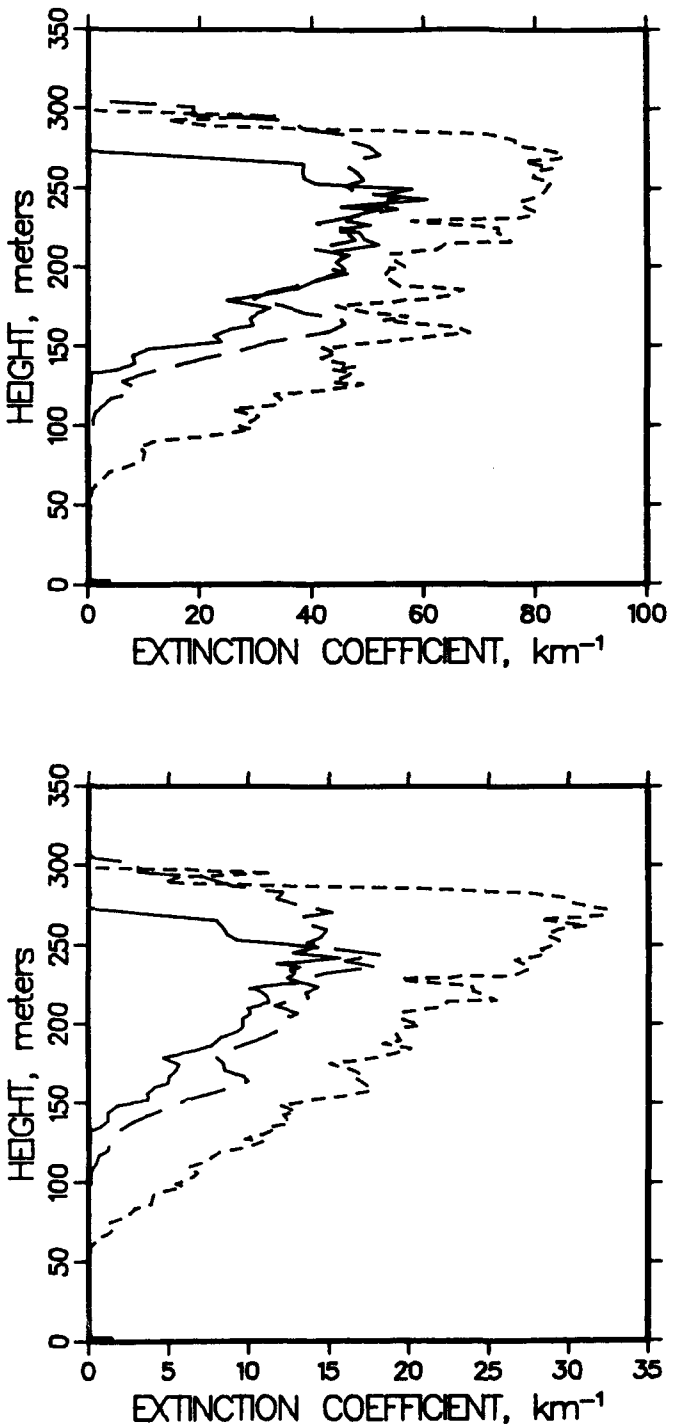

Figure 2. Extinction profiles from observed data for wavelengths of 4 μm (top) and 10.6 μm (bottom).

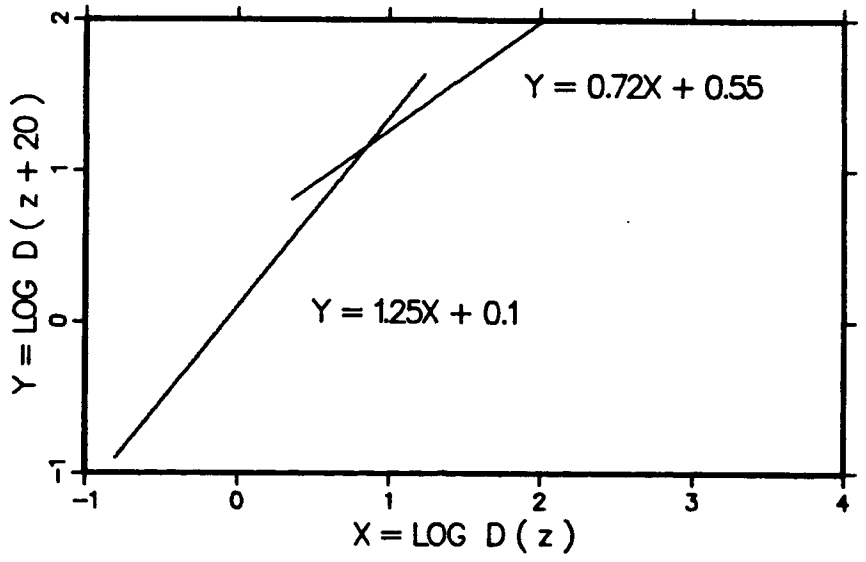

Figure 3. Relationship between the extinction coefficient (0.55 μm) at heights z and z + 20 m (after Duncan et al., 1980).

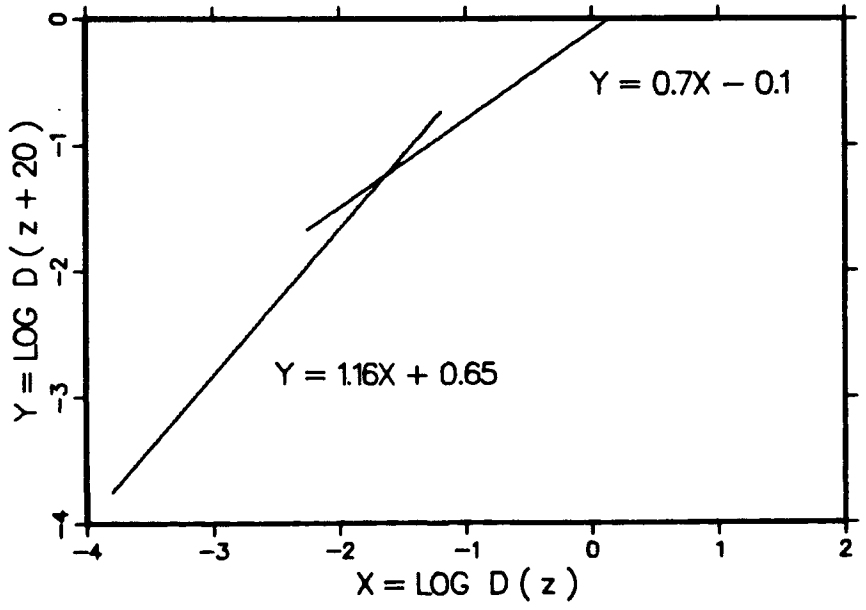

Figure 4. Relationship between liquid water content at heights z and z + 20 m (after Duncan et al., 1980).

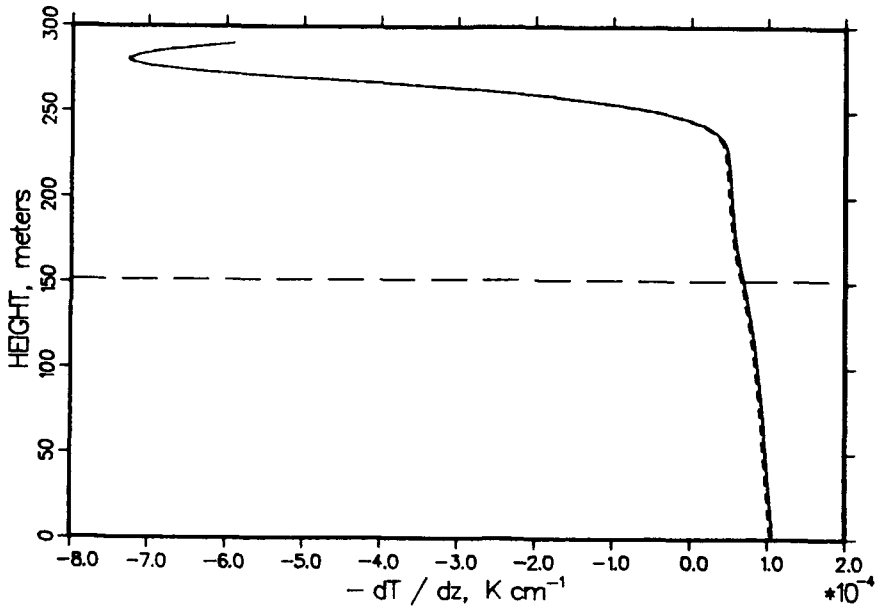

Figure 5a. Cluster and ambient air lapse rates for model profile 5. (Solid line: cluster; short-dashed line: ambient air; long-dashed line: height of inflection point of log (LWC) profile.)

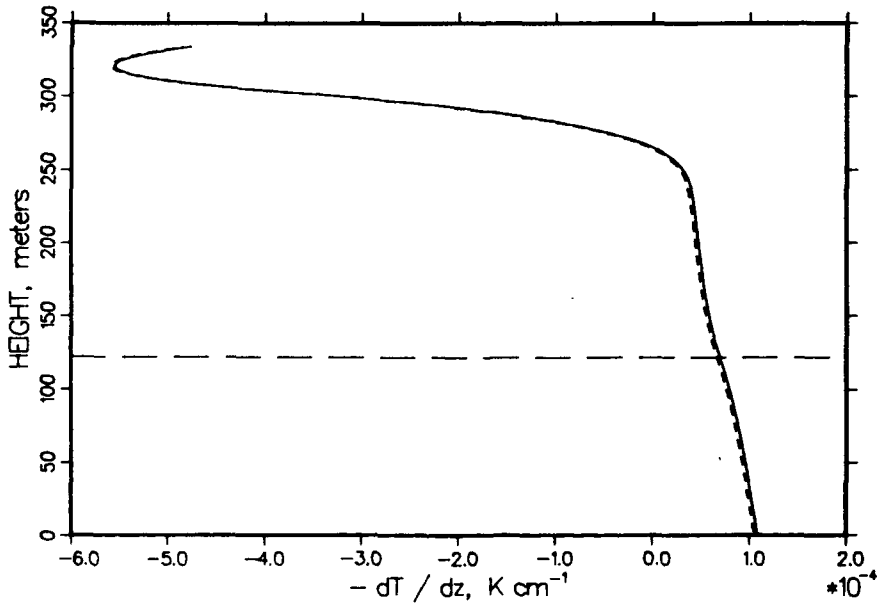

Figure 5b. Cluster and ambient air lapse rates for model profile 6. (Solid line: cluster; short-dashed line: ambient air; long-dashed line: height of inflection point of log (LWC) profile.)

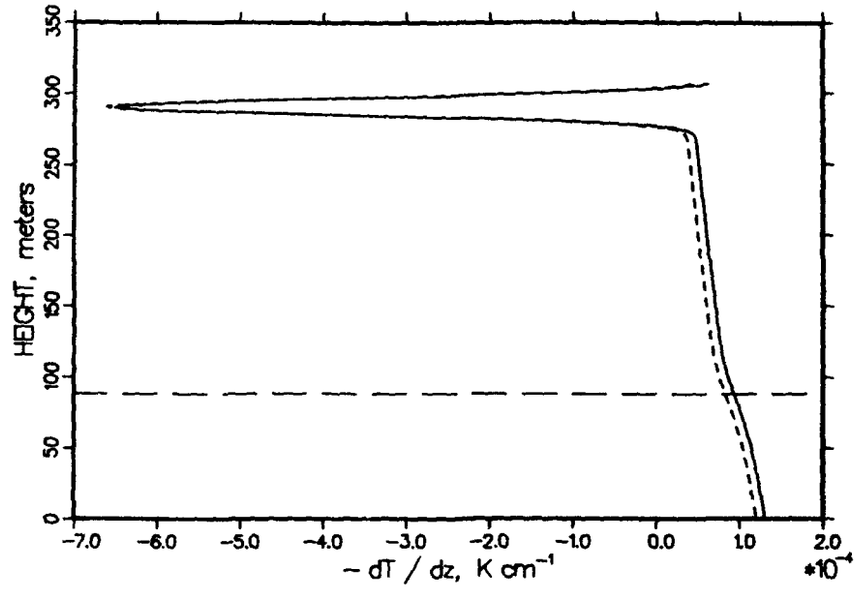

Figure 5c. Cluster and ambient air lapse rates for model profile 7. (Solid line: cluster; short-dashed line: ambient air; long-dashed line: height of inflection point of log (LWC) profile.)

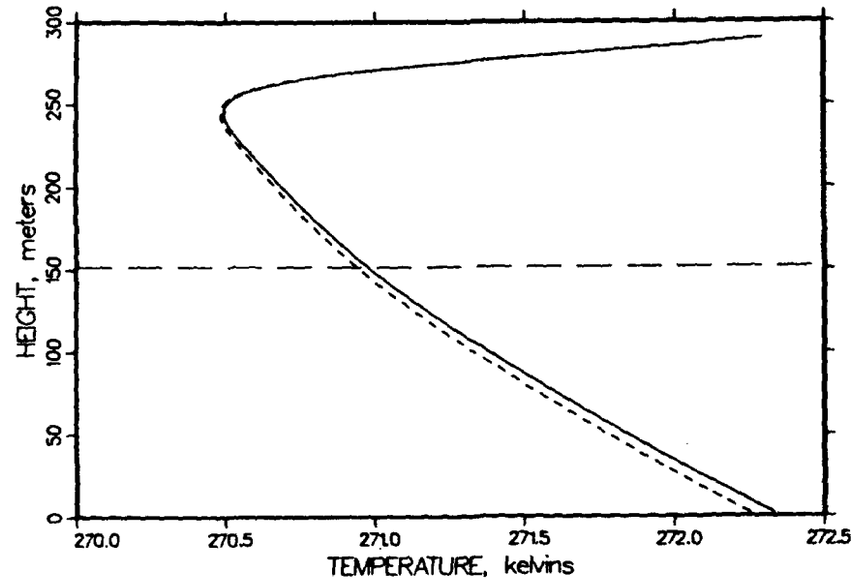

Figure 6a. Cluster and ambient temperature profiles for model profile 5. (Solid line: cluster; short-dashed line: ambient; long-dashed line: height of inflection point of log (LWC) profile.)

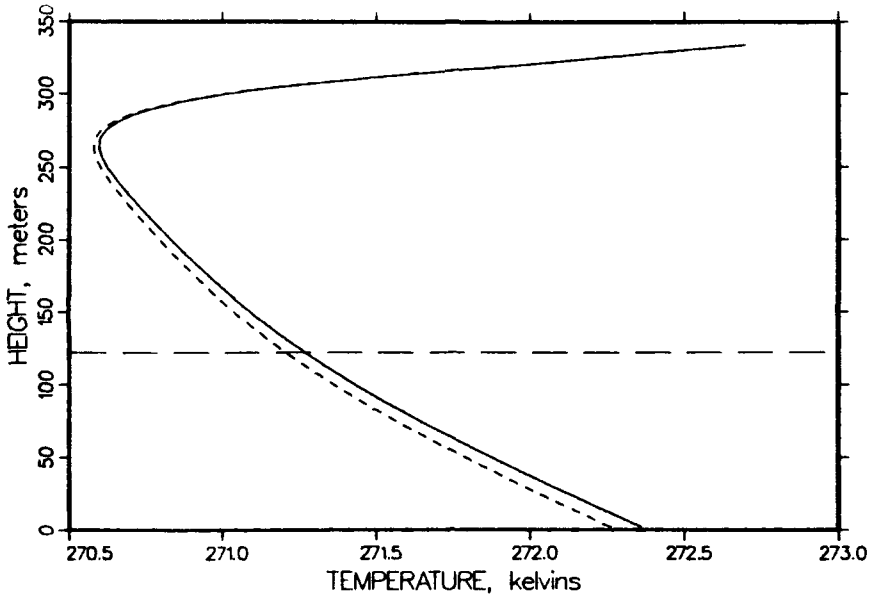

Figure 6b. Cluster and ambient temperature profiles for model profile 6. (Solid line: cluster; short-dashed line: ambient; long-dashed line: height of inflection point of log (LWC) profile.)

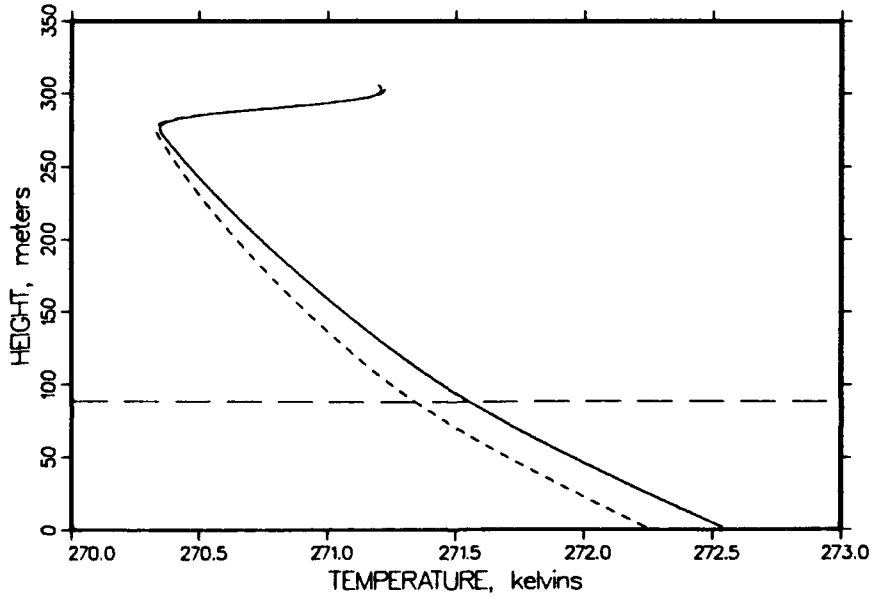

Figure 6c. Cluster and ambient temperature profiles for model profile 7. (Solid line: cluster; short-dashed line: ambient; long-dashed line: height of inflection point of log (LWC) profile.)

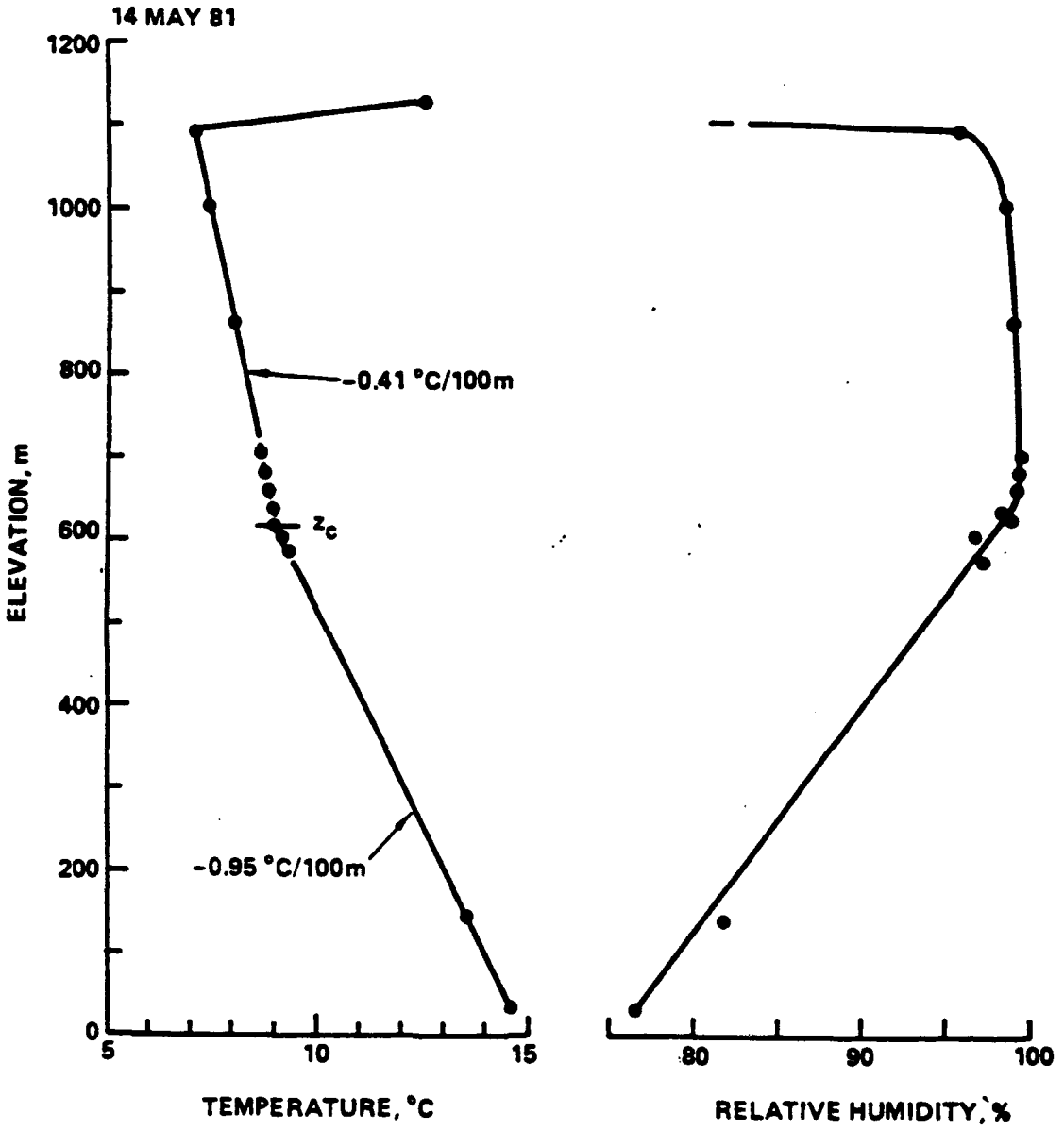

Figure 7. Ambient temperature and relative humidity profiles of marine stratus (Noonkester 1982).

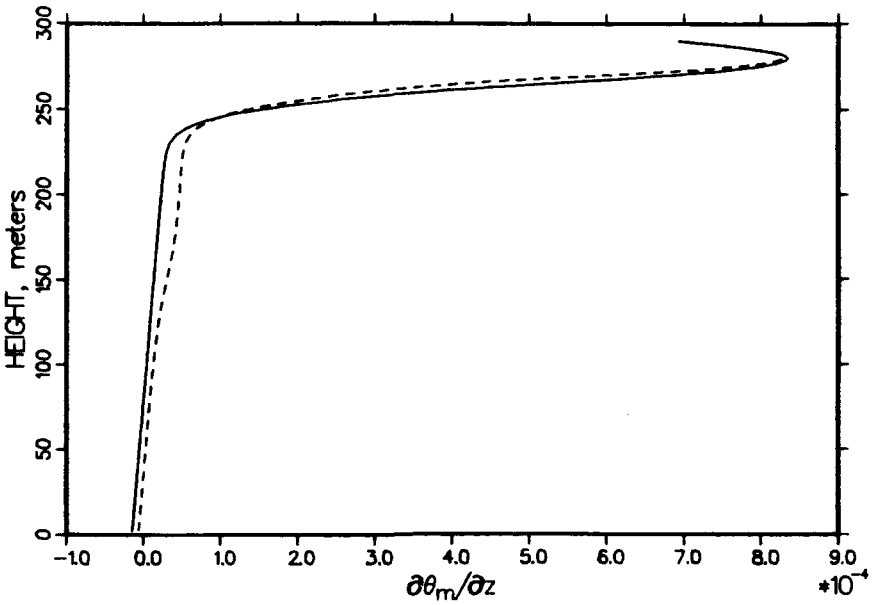

Figure 8a. Potential temperature profiles for model profile 5. (Solid line: cluster; dashed line: ambient air.)

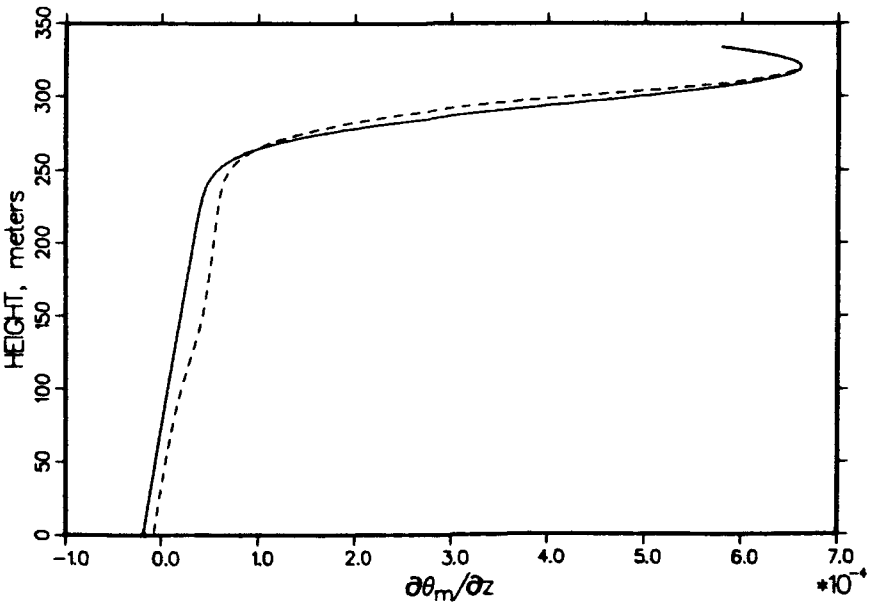

Figure 8b. Potential temperature profiles for model profile 6. (Solid line: cluster; dashed line: ambient air.)

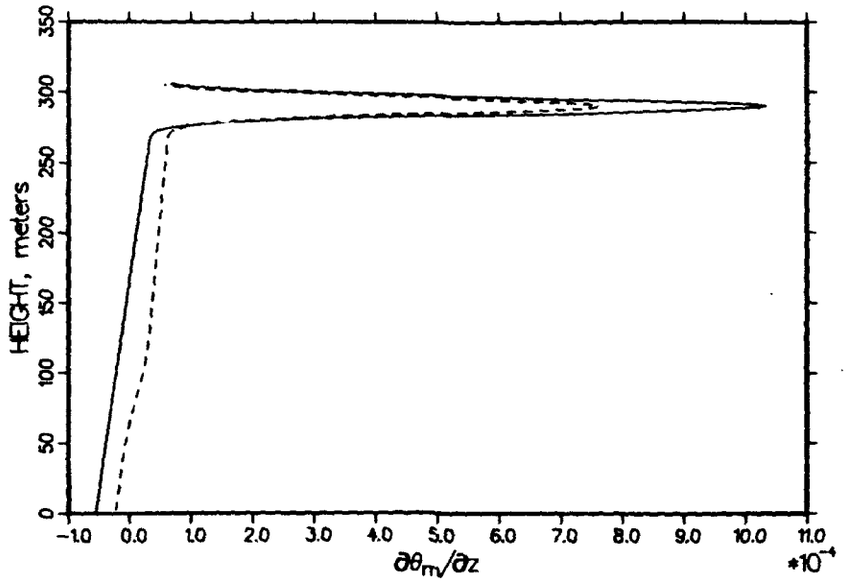

Figure 8c. Potential temperature profiles for model profile 7. (Solid line: cluster; dashed line: ambient air.)

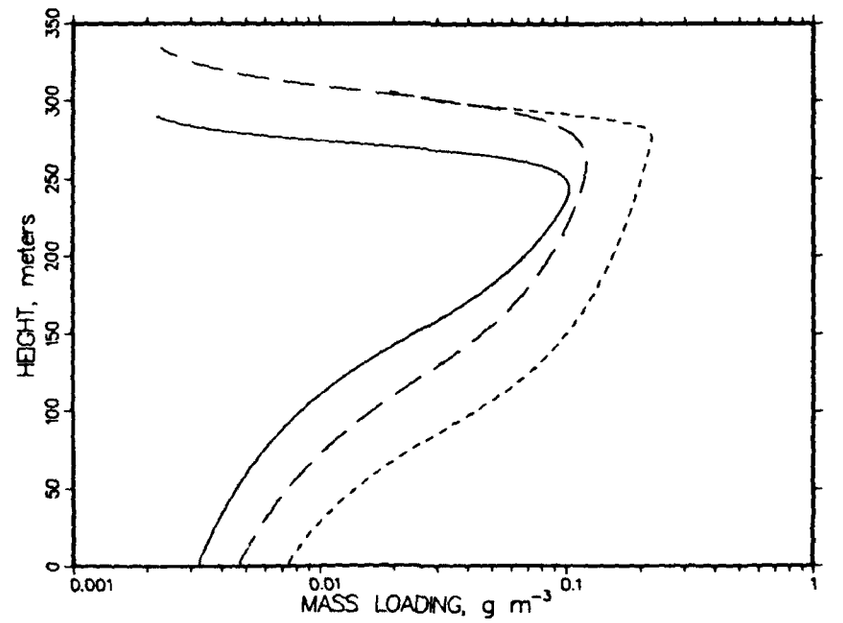

Figure 9. Model mass loading curves for model profiles. (Solid line: profile 5; long dashes: profile 6; short dashes: profile 7.)

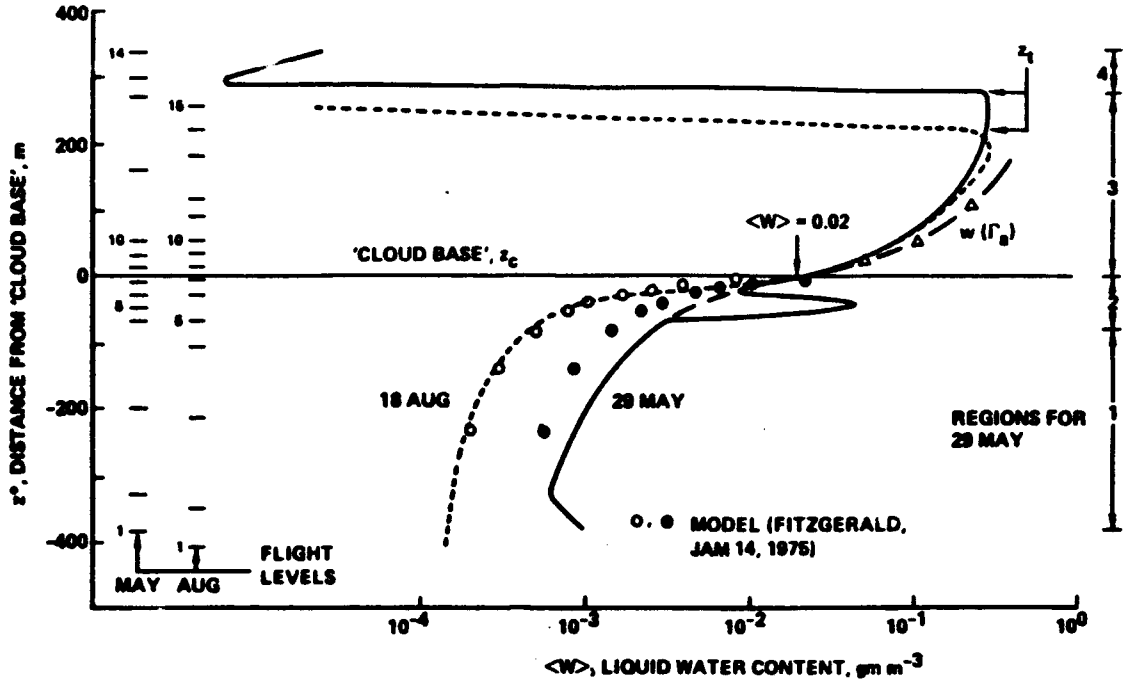

Figure 10. LWC profiles of Noonkester.

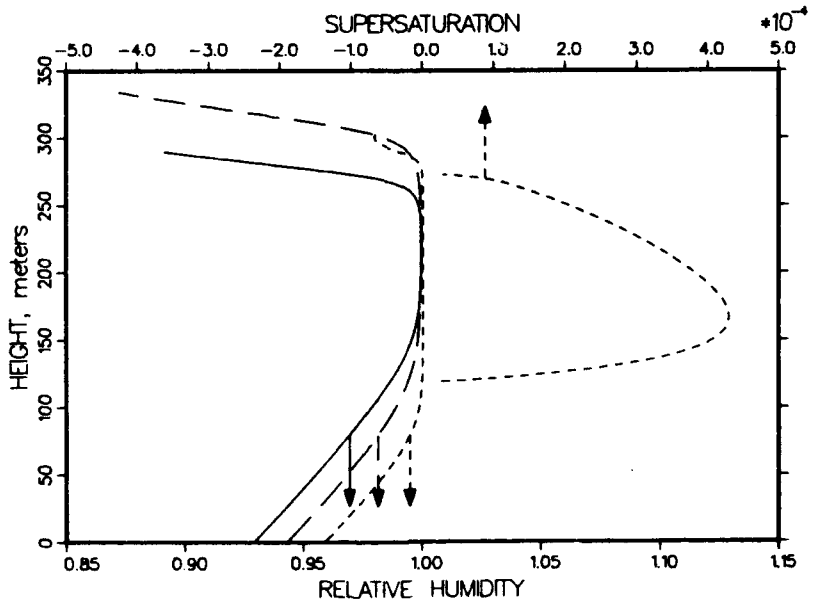

Figure 11. Model relative humidity profiles.
(Solid line: profile 5; long dashes: profile 6; short dashes: profile 7.)

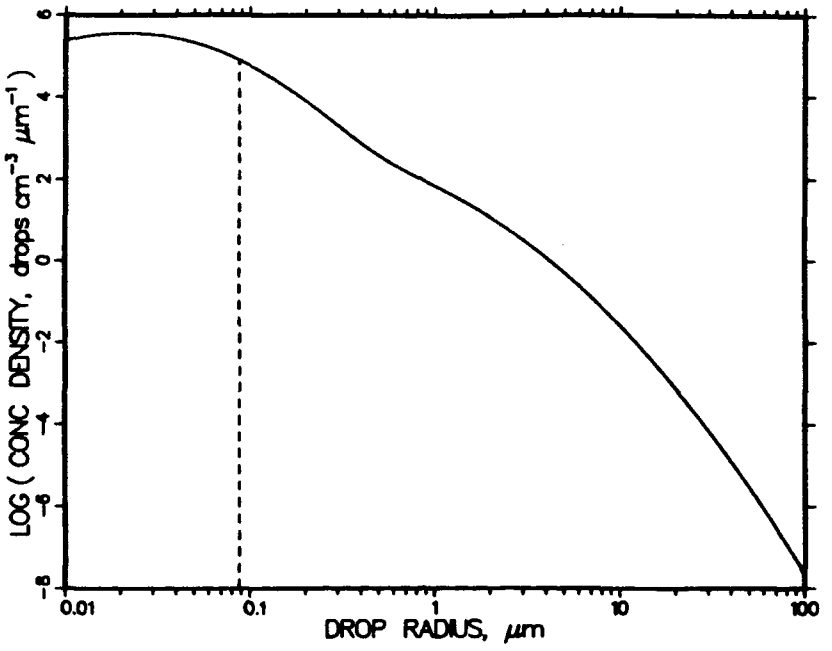

Figure 12a. Reference level drop size distribution (damp) for model profile 5.

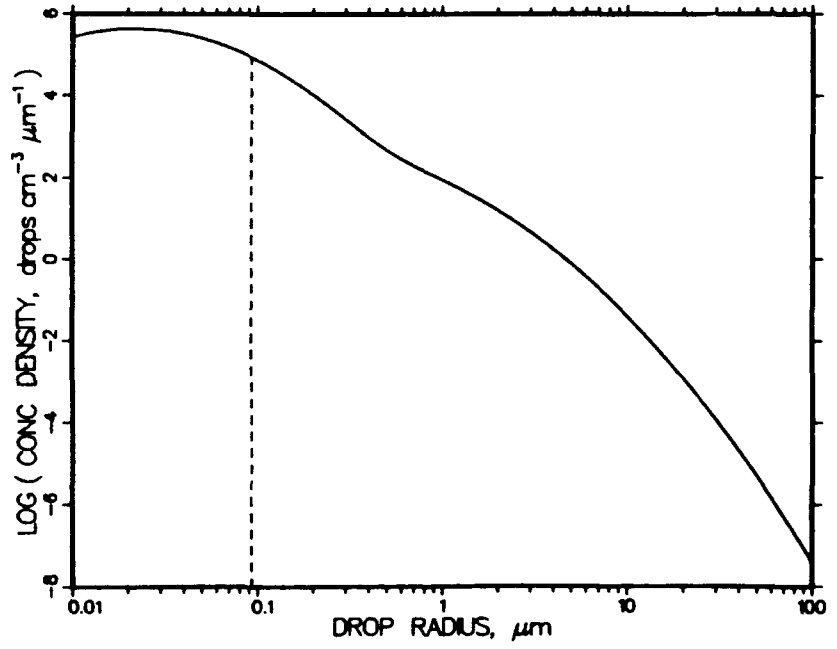

Figure 12b. Reference level drop size distribution (damp) for model profile 6.

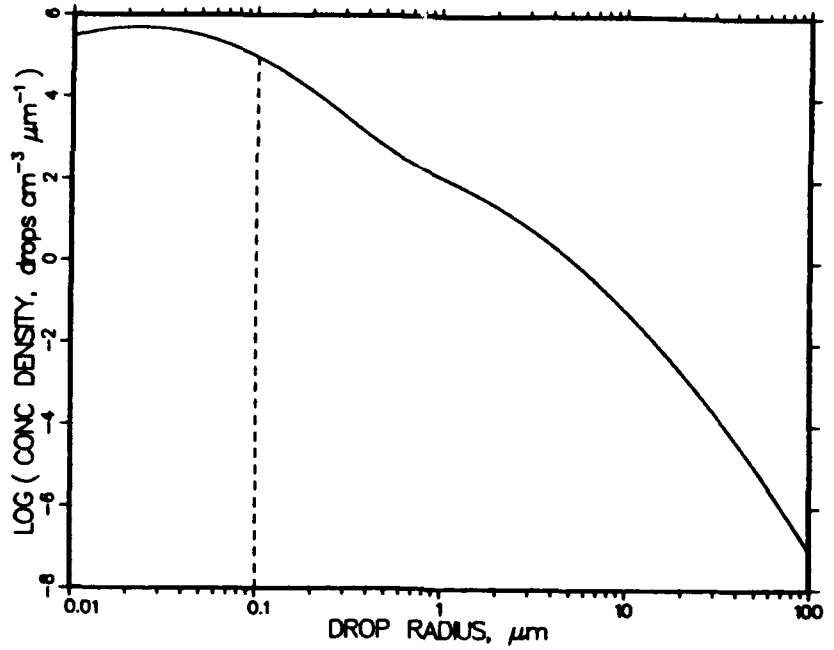

Figure 12c. Reference level drop size distribution (damp) for model profile 7.

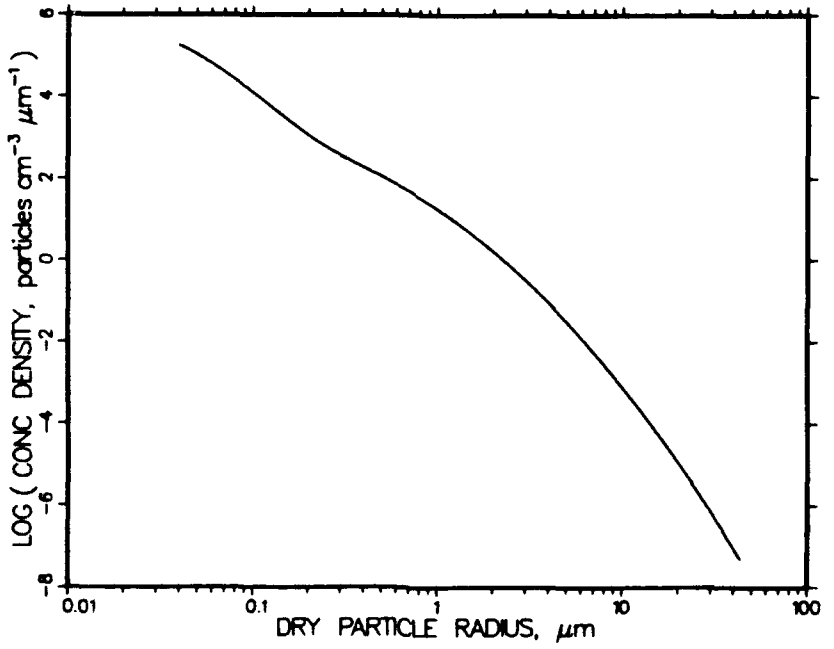

Figure 13a. Reference level dry particle size distribution for model profile 5.

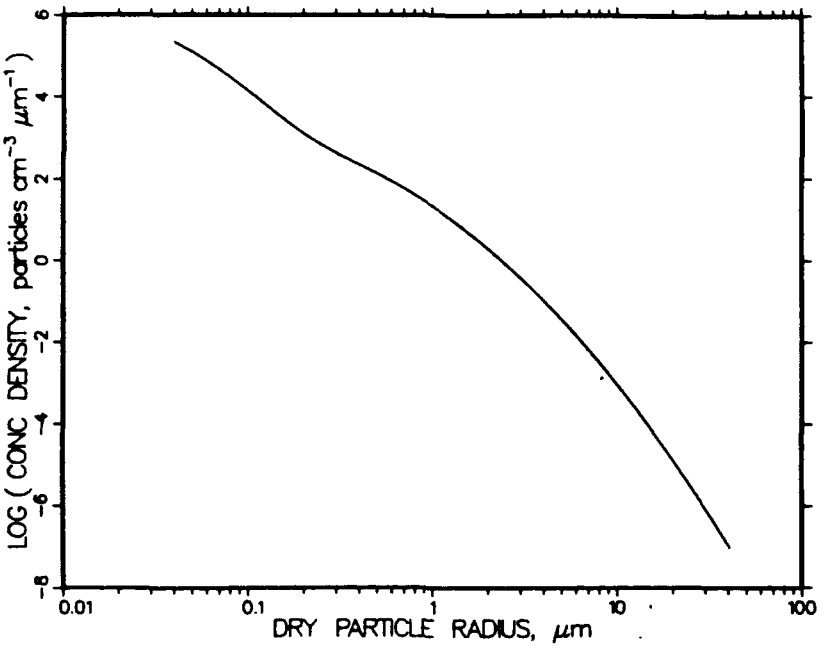

Figure 13b. Reference level dry particle size distribution for model profile 6.

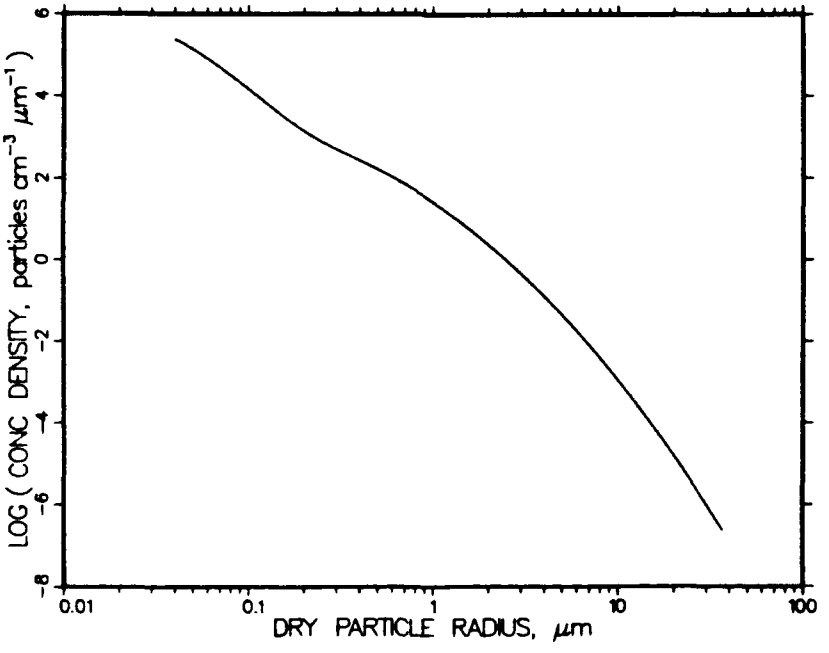

Figure 13c. Reference level dry particle size distribution for model profile 7.

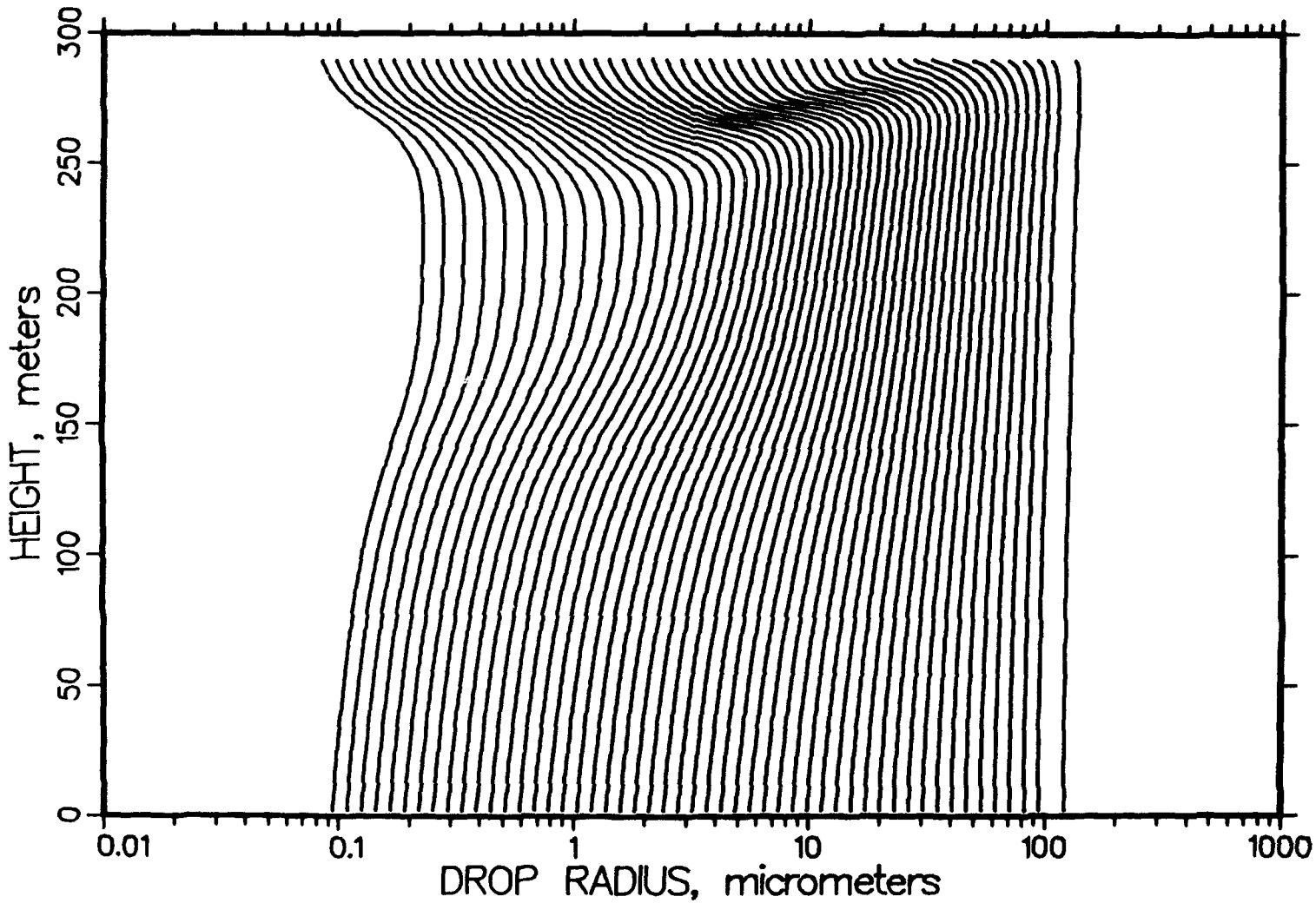

Figure 14a. Model drop size growth for profile 5.

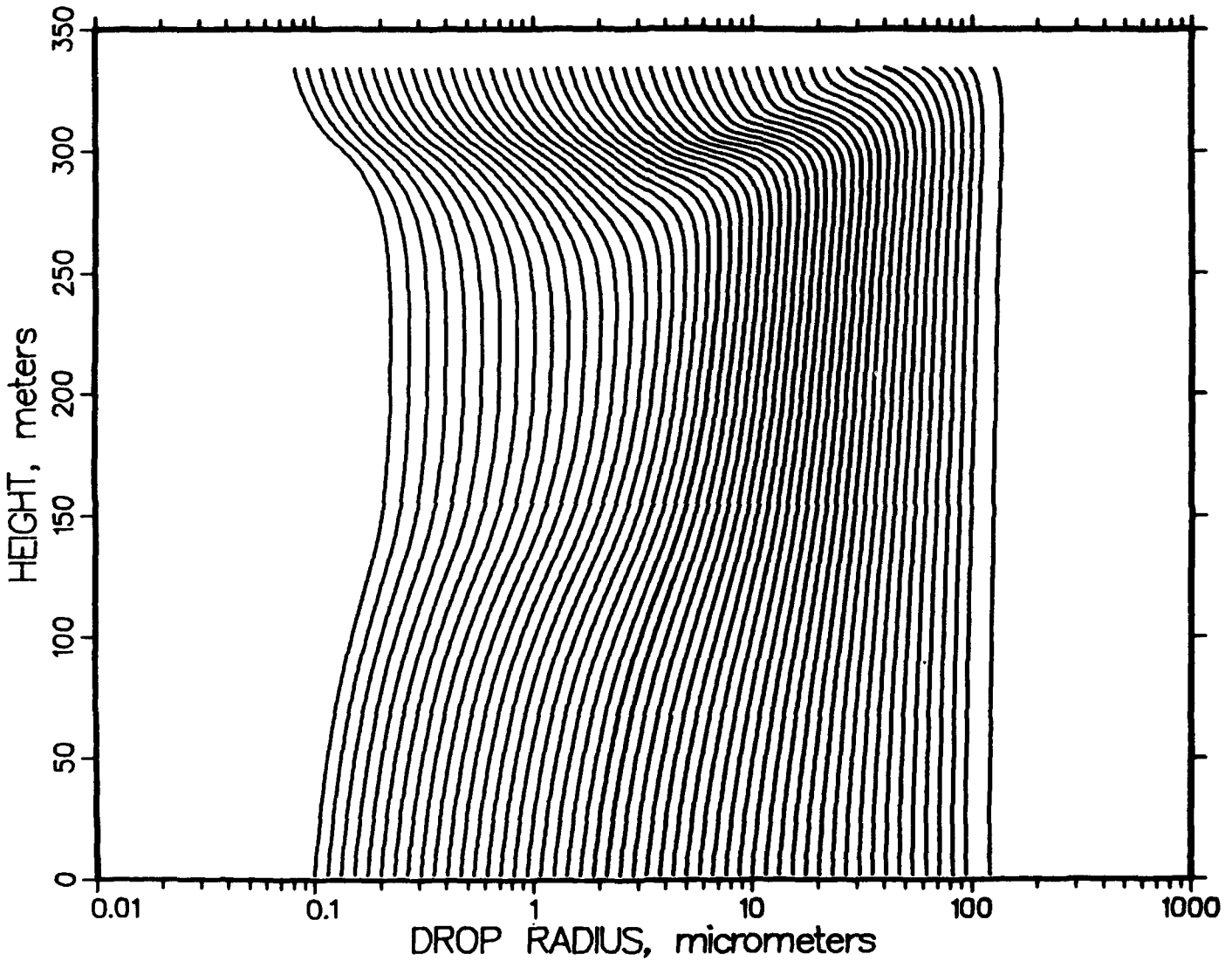

Figure 14b. Model drop size growth for profile 6.

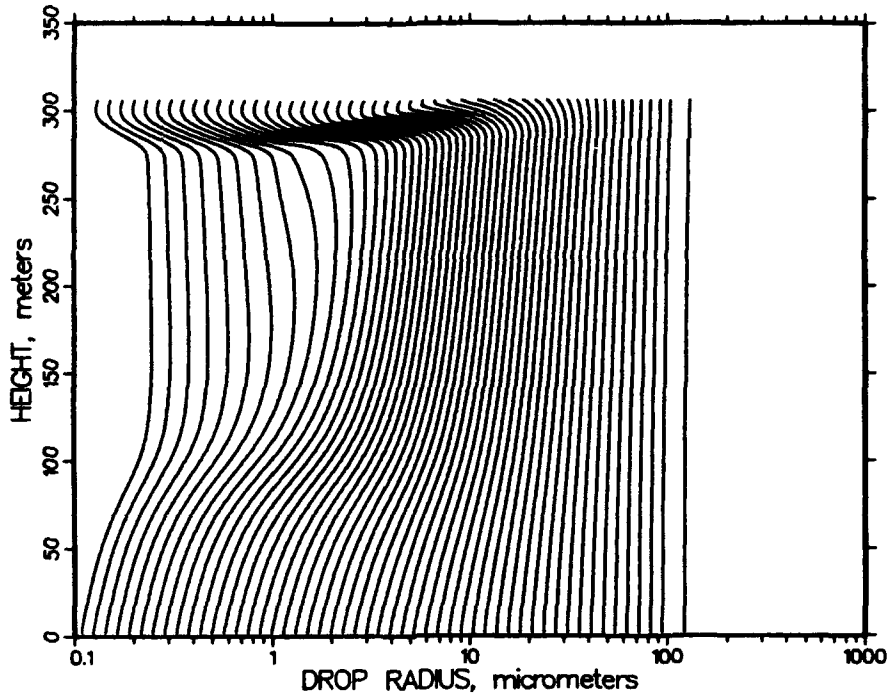

Figure 14c. Model drop size growth for profile 7.

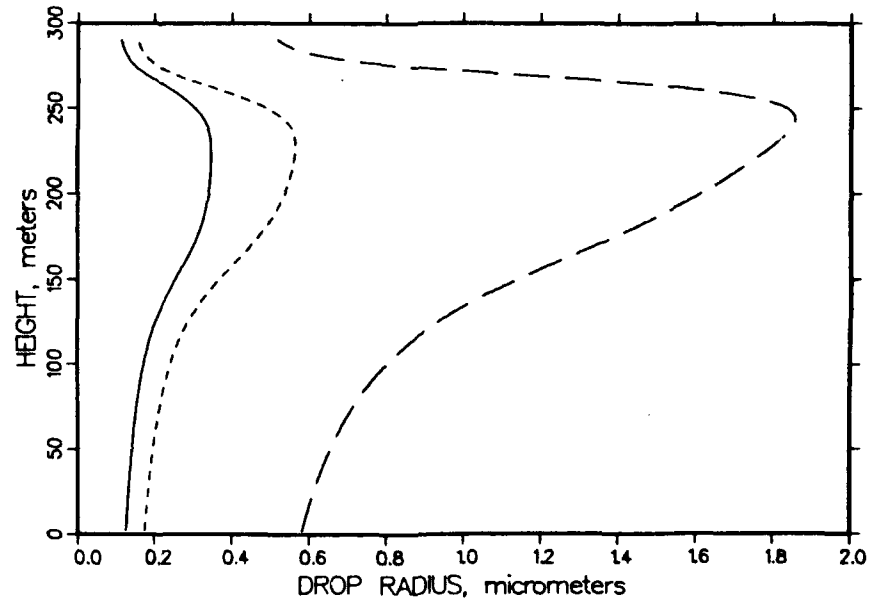

Figure 15a. Variation of average drop size with height for model profile 5. (Solid line: median radius; short-dashed line: mean radius; long-dashed line: mean volume radius.)

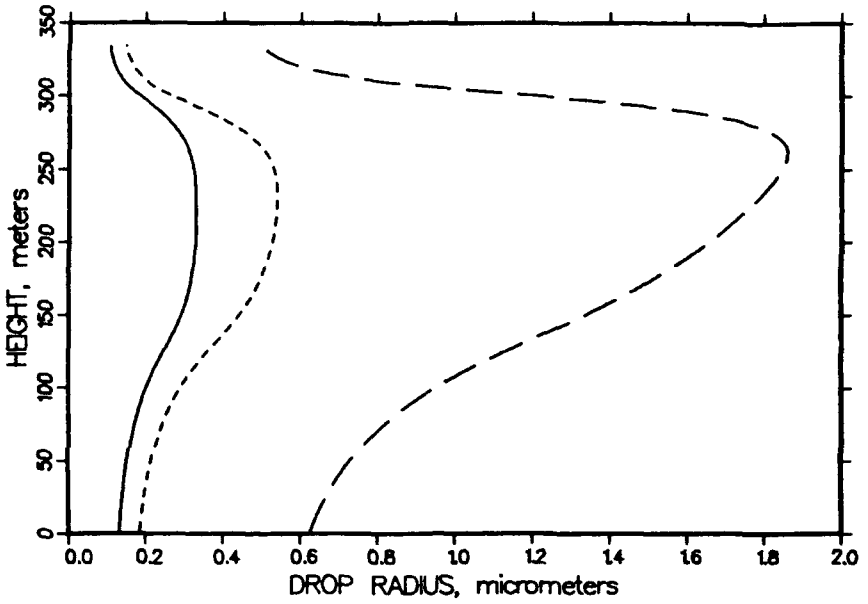

Figure 15b. Variation of average drop size with height for model profile 6. (Solid line: median radius; short-dashed line: mean radius; long-dashed line: mean volume radius.)

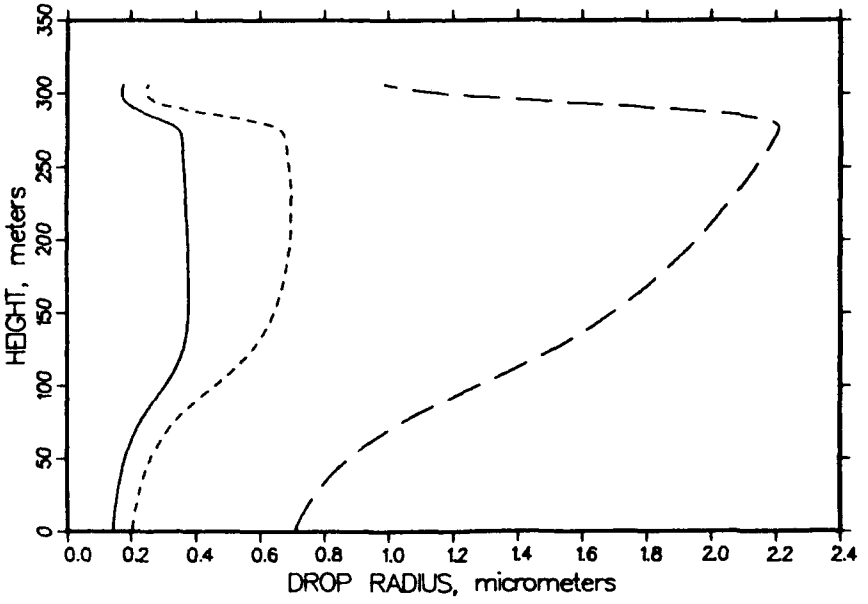

Figure 15c. Variation of average drop size with height for model profile 7. (Solid line: median radius; short-dashed line: mean radius; long-dashed line: mean volume radius.)

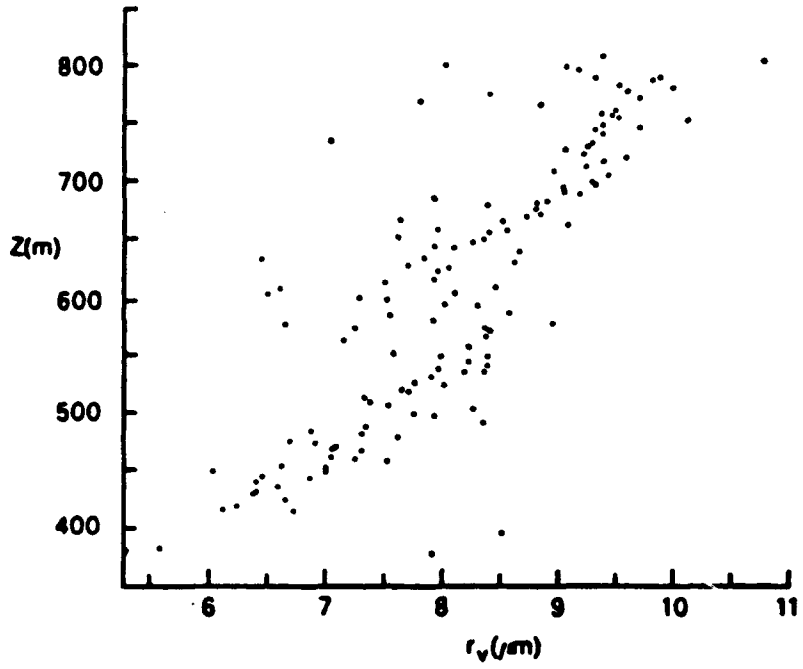

Figure 16. Mean volume radius vs height (Nicholls 1984).

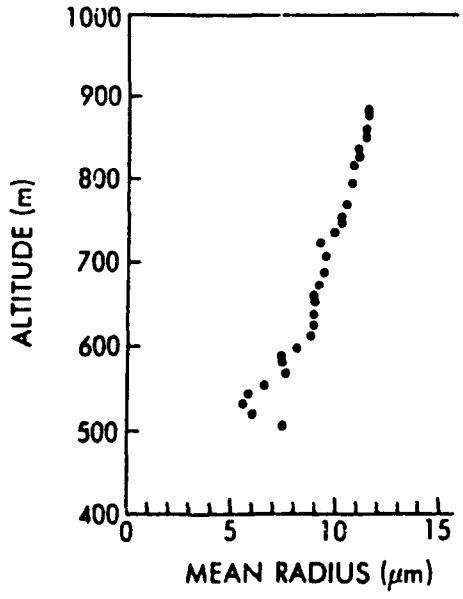

Figure 17. Mean radius vs height (Slingo et al. 1982b).

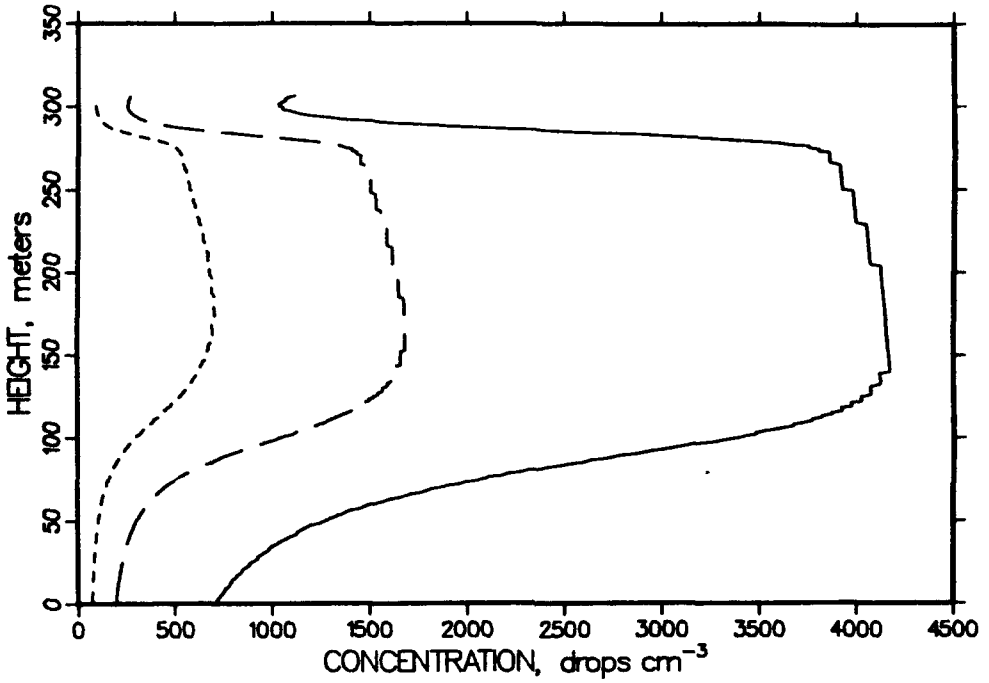

Figure 18. Model drop concentrations when lower cutoffs are *(right to left)* 0.25 μm, 0.5 μm, and 1.0 μm for profile 7.

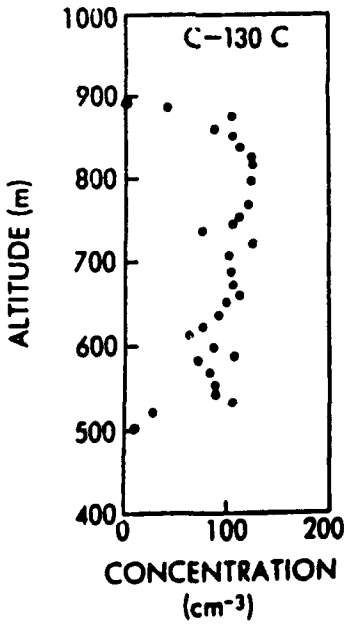

Figure 19. Drop concentration profile (Slingo et al. 1982b).

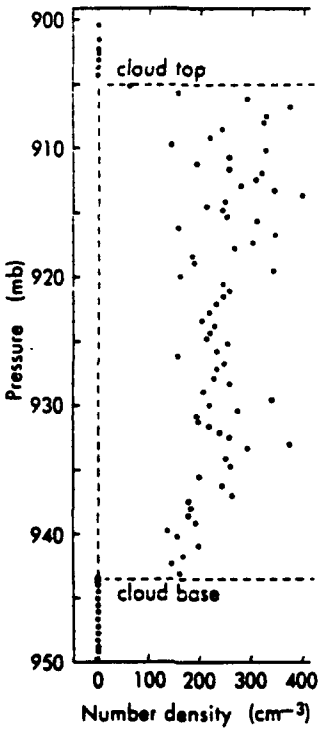

Figure 20. Drop concentration (Slingo et al. 1982a).

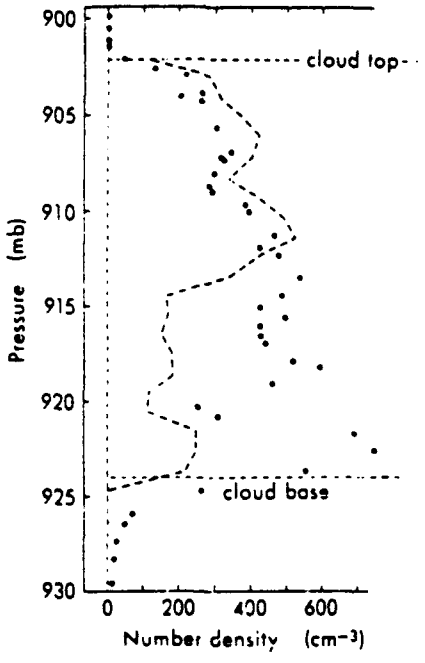

Figure 21. Drop concentration (Slingo et al. 1982a).

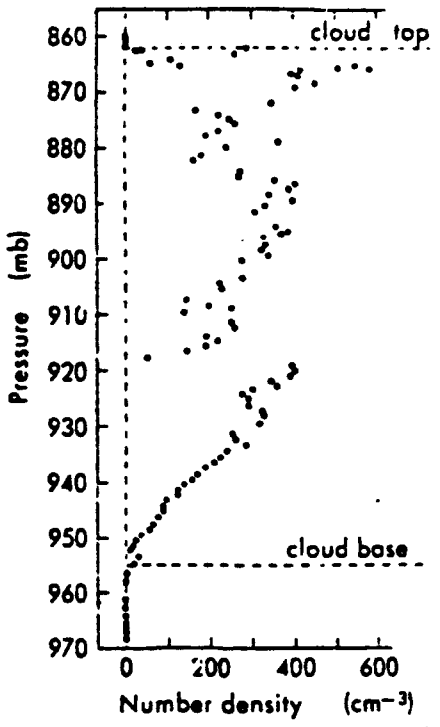

Figure 22. Drop concentration (Slingo et al. 1982a).

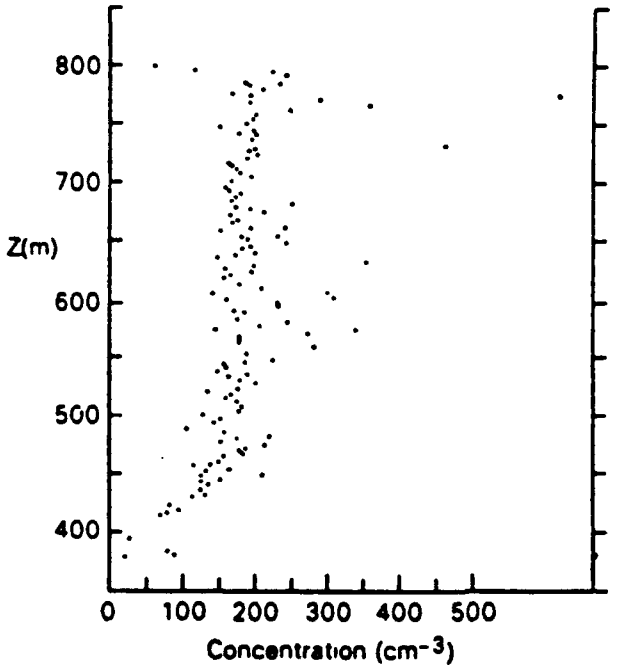

Figure 23. Drop concentration profile (Nicholls 1984).

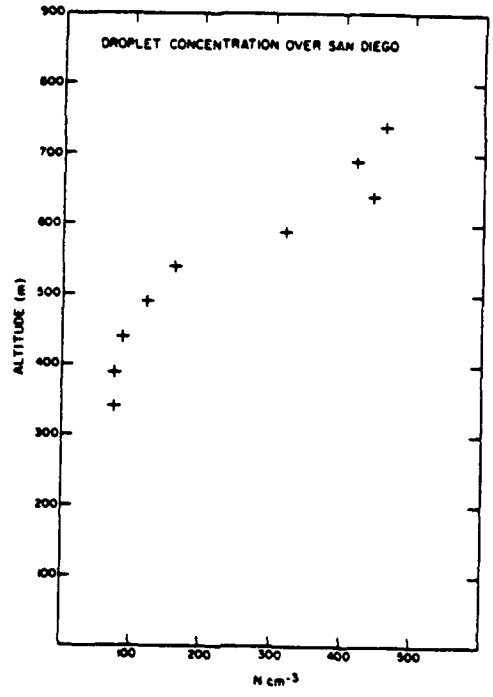

Figure 24. Drop concentration profile (Hudson 1983).

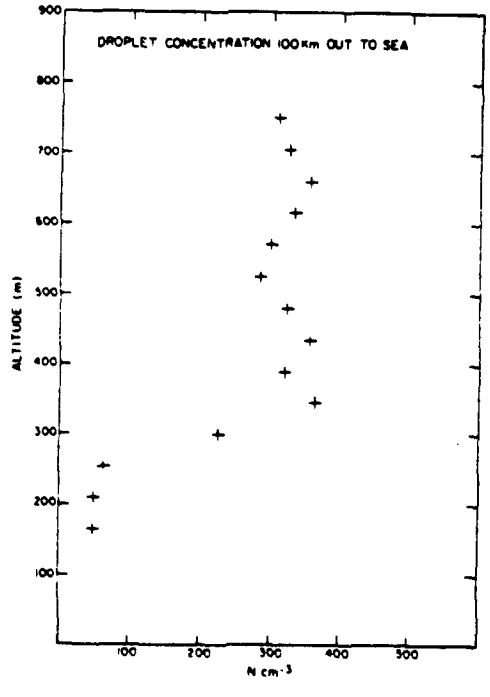

Figure 25. Drop concentration profile (Hudson 1983).

LITERATURE CITED

Baumgardner, D., 1985, Accuracy Analysis of the Forward Scattering Spectrometer Probe, Final Report Prepared for ASL Workshop on the Accuracy of the FSSP Probe, National Center for Atmospheric Research, Boulder, CO.

Borovikov, A. M., I. I. Gaivoronskii, E. G. Zak, et al., 1961, Fizika oblakov (Physics of Clouds), ed. by A. Kh. Khrgian, Leningrad, Gidrometeoizdat, p. 119, cited by Mao Jie-tai and Koo Chen-chao (date unknown).

Borovikov, A. M., A. K. Khrgian, et al., 1963, Cloud Physics, Trans. from Russian, Office of Technical Services, U.S. Dept. of Commerce, Washington, DC.

Clamen, A., and W. H. Gauvin, March 1969, "Effects of Turbulence on the Drag Coefficients of Spheres in a Supercritical Flow Regime," AIChE Journal **15** (2): 184-189.

Driedonks, A. G. M., and P. G. Duynkerke, 1989, "Current Problems in the Stratocumulus-Topped Atmospheric Boundary Layer," Boundary-Layer Meteorology **46**: 275-303.

Duncan, L. D., J. D. Lindberg, and R. B. Loveland, 1980, An Empirical Model of the Vertical Structure of German Fogs, ASL-TR-0071, U.S. Army Atmospheric Sciences Laboratory, White Sands Missile Range, NM.

Fitzgerald, J. W., W. A. Hoppel, and M. A. Vietti, 1982, "The Size and Scattering Coefficient of Urban Aerosol Particles at Washington, DC as a Function of Relative Humidity," J. of the Atmos. Sciences **39** (8): 1838-1852.

Goodman, J. K., 1976, The Microstructure of California Coastal Fog and Stratus, Report No. 76-09, Dept. of Meteorology, San Jose State University, San Jose, CA.

Hänel, G., 1976, "The Properties of Atmospheric Aerosol Particles as Functions of the Relative Humidity at Thermodynamic Equilibrium with the Surrounding Moist Air," Advances in Geophysics **19**: 73-188.

Hänel, G., 1984, "The Physical Chemistry of Atmospheric Particles," Workshop on Hygroscopic Aerosols in the Planetary Boundary Layer (Hygroscopic Aerosols), Eds. L. H. Ruhnke and A. Deepak.

Hänel, G., 1987, "The Role of Aerosol Properties during the Condensational Stage of Cloud: A Reinvestigation of Numerics and Microphysics," Contributions to Atmospheric Physics (Beiträge zur Physik der Atmosphäre), **60** (3): 321-339.

Hänel, G., and M. Lehmann, 1981, "Equilibrium Size of Aerosol Particles and Relative Humidity: New Experimental Data from Various Aerosol Types and Their Treatment for Cloud Physics Application," Contributions to Atmospheric Physics (Beiträge zur Physik der Atmosphäre), **54** (1): 57-71.

Harrison, 1965, cited by G. Hänel., 1976.

Heaps, Melvin G., 1982, A Vertical Structure Algorithm For Low Visibility/Low Stratus Conditions, ASL-TR-0111, U.S. Army Atmospheric Sciences Laboratory, White Sands Missile Range, NM.

Hudson, J. G., 1983, "Effects of CCN Concentrations on Stratus Clouds," J. of the Atmos. Sciences **40** (2): 480-486.

Hudson, J. G., 1984, "CCN Measurements Within Clouds," American Meteorological Society: 0001-0010.

Hudson, J. G., 1985, Accuracy of FSSP Viewed from FCN and CCN Perspective, Final Report Prepared for ASL Workshop on the Accuracy of the FSSP Probe, Atmospheric Sciences Center, Desert Research Institute, Reno, NV.

Hudson, J. G., and C. F. Rogers, 1986, "Relationship Between Critical Supersaturation and Cloud Droplet Size: Implications for Cloud Mixing Processes," American Meteorological Society, **43** (21): 2341-2359.

Husar, R. B., and J. M. Holloway, 1984, "The Properties and Climate of Atmospheric Haze," Workshop on Hygroscopic Aerosols in the Planetary Boundary Layer (Hygroscopic Aerosols), Eds. L. H. Ruhnke and A. Deepak.

Kao, C. J., and T. Yamada, 1989, "Numerical Simulations of a Stratocumulus-Capped Boundary Layer Observed over Land," J. of the Atmos. Sciences, **46** (6): 832-848.

Kilmer, Neal H., 1992, Unified Very Low Stratus Cloud/Subcloud Microphysics Model: User's Guide, to be written as a contractor's technical report, Physical Science Laboratory, New Mexico State University.

Korolev, A. V., I. P. Mazin, YU. YE. Makarov, and V. S. Novikov, (1987 trans.), Droplet Size Distribution in Stratiform Clouds, Translation Services, Reference Library Branch, Washington, DC.

Lala, G. G., D. R. Fitzgerald, and M. B. Meyer, 1987, Fog, Rain, and Aerosol Attenuation in the Atmosphere, Final Report, Atmospheric Sciences Research Center, State University of New York at Albany.

Lindberg, James D., 1982, Early Wintertime European Fog and Haze; Report on Project Meppen 80, ASL-TR-0108, U.S. Army Atmospheric Sciences Laboratory, White Sands Missile Range, NM.

Lindberg, James D., 1984, Final Report on the European Vertical Structure Experiment at Cardington, England, ASL-TR-0153, U.S. Army Atmospheric Sciences Laboratory, White Sands Missile Range, NM.

Lindberg, James D., and L. D. Duncan, 1985, Improving the EOSAEL Vertical Structure Algorithm Fit to Measured Data, ASL-TR-0168, U.S. Army Atmospheric Sciences Laboratory, White Sands Missile Range, NM.

Loveland, R. B., and J. D. Lindberg, 1988, "Problems in Comparing Particulate Spectrometer and Visibility Meter Data," Applied Optics **27**, 4318.

Low, D. H., 1980, One-Dimensional Cloud Microphysical Models for Central Europe and Their Optical Properties, ASL-TR-0070, U.S. Army Atmospheric Sciences Laboratory, White Sands Missile Range, NM,

Lowe, P. R., and J. M. Ficke, 1974, "Technical Paper," Environmental Prediction Res. Facility, Naval Post Grad. School, Monterey, CA, 4-74. (Cited by Pruppacher and Klett, 1980.)

Mao, Jie-tai, and Chen-chao Koo, 1963, "VI. Superadiabatic Concentration of Water Content in Layer Clouds," in Koo Chen-chao, et al., Some Theoretical Problems Concerning the Microphysical Processes of Precipitation, Cloud, and Fog, AFCRL-68-0665 (Dec. 1968). Translation No. 39, Air Force Cambridge Research Laboratories, L. G. Hanscom Field, Bedford, MA, pp. 77-85. Translated from Institute of Geophysics and Meteorology, Academia Sinica, Peking, China 1963, by Oriental Library, Research Language Center, Emmanuel College.

Neve, R. S., March 1986, "The Importance of Turbulence Macroscale in Determining the Drag Coefficient of Spheres," International J. of Heat and Fluid Flow **7** (1): 28-36, Butterworth and Co. Ltd.

Nicholls, S., 1984, "The Dynamics of Stratocumulus: Aircraft Observations and Comparisons with a Mixed Layer Model," J. Royal Met. Soc. **110**: 783-820.

Noonkester, V. R., 1982, Aerosol and Humidity Structure Beneath Maritime Stratus Clouds, NOSC TR 783, Naval Ocean Systems Center, San Diego, CA 92152.

Noonkester, V. Ray, 1984, "Droplet Spectra Observed in Marine Stratus Cloud Layers," J. of the Atmos. Sciences **41** (5): 829-845.

Obukhov, A. M., 1971, "Turbulence in an Atmosphere with a Nonuniform Temperature," Boundary-Layer Meteorology **2**: 7-29.

Priestley, C. H. B., 1953, "Buoyant Motion in a Turbulent Environment," Australian J. of Physics **6**: 279-290.

Pruppacher, H. R., and J. D. Klett, 1978, 1980, Microphysics of Clouds and Precipitation, D. Reidel Publishing Co., Dordrecht, Holland.

Rachele, H., and N. H. Kilmer, 1991, A Derivation for Determining Double Exponential Liquid Water Content and Extinction Profiles from Discrete Data, Technical Report ASL-TR-0290, U.S. Army Atmospheric Sciences Laboratory, White Sands Missile Range, NM.

Rogers, C. William, J. T. Hanley, and E. J. Mack, 1985, Updating the Smith-Feddes Model, Calspan Final Report No. 7330-1, Calspan Corporation, P.O. Box 400, Buffalo, NY 14225.

Rogers, R. R., 1979, A Short Course in Cloud Physics, 2nd Ed., (International Series in Natural Philosophy: V. 96), Pergamon Press, Oxford, England; Elmsford, N.Y.; Willowdale, Ontario, Canada; Potts Point, N.S.W., Australia; Paris, France; Federal Republic of Germany.

Rogers, R. R., and M. K. Yau, 1989, A Short Course in Cloud Physics, 3rd Ed., (International Series in Natural Philosophy: V. 113), Pergamon Press, Oxford, England.

Shettle, E. P., and R. W. Fenn, 1979, Models for the Aerosols of the Lower Atmosphere and the Effects of Humidity Variations on Their Optical Properties, AFGL-TR-79-0214, Air Force Geophys. Lab., Hanscom AFB, MA 01731.

Singleton, F., and D. J. Smith, 1960, "Some Observations of Drop-Size Distributions in Low Layer Clouds," J. Royal Met. Soc.: 454-467.

Slingo, A., R. Brown, and C. L. Wrench, 1982a, "A Field Study of Nocturnal Stratocumulus; III. High Resolution Radiative and Microphysical Observations," J. Royal Met. Soc. **108**: 145-165.

Slingo, A., S. Nicholls, and J. Schmetz, 1982b, "Aircraft Observations of Marine Stratocumulus during Joint Air-Sea Interaction Experiment (JASIN)," J. Royal Met. Soc. **108**: 833 856.

Warner, J., 1970, "On Steady-State One-Dimensional Models of Cumulus Convection," J. of the Atmos. Sciences **27** (7): 1035-1040.

APPENDIX

HYDROSTATIC APPROXIMATION

Assumptions:

a. Hydrostatic approximation is based on TOTAL pressure (contributions from both dry air and water vapor) in the ENVIRONMENT (ambient air outside of parcel).

b. TOTAL pressure inside parcel equals TOTAL pressure in the environment at the same height.

Thus, if P is defined to be total pressure,

$$P = P_d + e = P_d' + e' \qquad (A-1)$$

$$P = P_d\left(1 + \frac{W_v}{\varepsilon}\right) = P_d'\left(1 + \frac{W_v'}{\varepsilon}\right), \qquad (A-2)$$

where $\varepsilon = 0.621972$

$$P_d' = \frac{P}{\left(1 + \frac{W_v'}{\varepsilon}\right)} \qquad (A-3)$$

$$\frac{dP}{dz} = -g\rho'_{total} = -g\left(\rho'_a + W_v'\rho'_a\right) = -g\rho'_a\left(1 + W_v'\right) = \frac{-gP_d'\left(1 + W_v'\right)}{R_dT'} \qquad (A-4)$$

The ideal gas law is used in substituting for ρ_a'

Substituting equation (A-3) into equation (A-4) yields

$$\frac{dP}{dz} = \frac{-gP}{R_dT'}\left(\frac{1 + W_v'}{1 + W_v'/\varepsilon}\right) \qquad (A-5)$$

Dividing both sides by P, multiplying both sides by dz, and integrating produces

$$\ln P_i - \ln P_{i-1} \doteq \frac{-g}{R_d\overline{T}'}\left(\frac{1 + \overline{W}_v'}{1 + \overline{W}_v'/\varepsilon}\right)\Delta z \qquad (A-6)$$

where P_i is the total pressure at level i, P_{i-1} is the total pressure at level i-1, and Δz is the difference in heights of the two levels $(z_i - z_{i-1})$.

T' and W_v' are functions of z but are approximated by the constants, $\overline{T}'$ and $\overline{W}_v'$, respectively, to facilitate integration. The smallness of the fractional changes in T' and in the fraction involving W_v' makes this a reasonable approximation.

Equation (A-6) leads quickly to

$$P_i \doteq P_{i-1}\exp\left[\frac{-g}{R_d\overline{T}'}\left(\frac{1 + \overline{W}_v'}{1 + \overline{W}_v'/\varepsilon}\right)\Delta z\right] \qquad (A-7)$$

Sometimes it is desirable to have an expression to replace dP_d/dz. From equation (A-2),

$$P_d\left(1+\frac{W_v}{\varepsilon}\right) = P \qquad (A-8)$$

$$\left(1+\frac{W_v}{\varepsilon}\right)\frac{dP_d}{dz} + \frac{P_d}{\varepsilon}\frac{dW_v}{dz} = \frac{dP}{dz} \qquad (A-9)$$

Using equation (A-5) to substitute for dP/dz and then substituting for P according to equation (A-8) and dividing both sides by $(1 + W_v/\varepsilon)$ produces

$$\frac{dP_d}{dz} = \frac{-gP_d}{R_dT'}\left(\frac{1+W_v'}{1+W_v'/\varepsilon}\right) - \left(\frac{P_d}{\varepsilon+W_v}\right)\frac{dW_v}{dz} \quad . \qquad (A-10)$$

If desired, the right-hand side of equation (A-5) can be expressed as $\frac{-gP}{R_dT_v'}$, where T_v' is the virtual temperature in the environment. Similarly, $\overline{T}_v'$ and T_v' can be used in equations (A-7) and (A-10).

DISTRIBUTION LIST FOR PUBLIC RELEASE

Commandant
U.S. Army Chemical School
ATTN: ATZN-CM-CC (S. Barnes)
Fort McClellan, AL 36205-5020

Commander
U.S. Army Aviation Center
ATTN: ATZQ-D-MA
Mr. Oliver N. Heath
Fort Rucker, AL 36362

Commander
U.S. Army Aviation Center
ATTN: ATZQ-D-MS (Mr. Donald Wagner)
Fort Rucker, AL 36362

NASA/Marshall Space Flight Center
Deputy Director
Space Science Laboratory
Atmospheric Sciences Division
ATTN: E501 (Dr. George H. Fichtl)
Huntsville, AL 35802

NASA/Marshall Space Flight Center
Atmospheric Sciences Division
ATTN: Code ED-41
Huntsville, AL 35812

Deputy Commander
U.S. Army Strategic Defense Command
ATTN: CSSD-SL-L
Dr. Julius Q. Lilly
P.O. Box 1500
Huntsville, AL 35807-3801

Commander
U.S. Army Missile Command
ATTN: AMSMI-RD-AC-AD
Donald R. Peterson
Redstone Arsenal, AL 35898-5242

Commander
U.S. Army Missile Command
ATTN: AMSMI-RD-AS-SS
Huey F. Anderson
Redstone Arsenal, AL 35898-5253

Commander
U.S. Army Missile Command
ATTN: AMSMI-RD-AS-SS
B. Williams
Redstone Arsenal, AL 35898-5253

Commander
U.S. Army Missile Command
ATTN: AMSMI-RD-DE-SE
Gordon Lill, Jr.
Redstone Arsenal, AL 35898-5245

Commander
U.S. Army Missile Command
Redstone Scientific Information Center
ATTN: AMSMI-RD-CS-R/Documents
Redstone, Arsenal, AL 35898-5241

Commander
U.S. Army Intelligence Center and Fort Huachuca
ATTN: ATSI-CDC-C (Mr. Colanto)
Fort Huachuca, AZ 85613-7000

Northrup Corporation
Electronics Systems Division
ATTN: Dr. Richard D. Tooley
2301 West 120th Street, Box 5032
Hawthorne, CA 90251-5032

Commander - Code 3331
Naval Weapons Center
ATTN: Dr. Alexis Shlanta
China Lake, CA 93555

Commander
Pacific Missile Test Center
Geophysics Division
ATTN: Code 3250 (Terry E. Battalino)
Point Mugu, CA 93042-5000

Lockheed Missiles & Space Co., Inc.
Kenneth R. Hardy
Org/91-01 B/255
3251 Hanover Street
Palo Alto, CA 94304-1191

Commander
Naval Ocean Systems Center
ATTN: Code 54 (Dr. Juergen Richter)
San Diego, CA 92152-5000

Meteorologist in Charge
Kwajalein Missile Range
P.O. Box 67
APO San Francisco, CA 96555

U.S. Department of Commerce
Mountain Administration Support
Center
Library, R-51 Technical Reports
325 S. Broadway
Boulder, CO 80303

Dr. Hans J. Liebe
NTIA/ITS S 3
325 S. Broadway
Boulder, CO 80303

NCAR Library Serials
National Center for Atmos Rsch
P.O. Box 3000
Boulder, CO 80307-3000

Bureau of Reclamation
ATTN: D: 1200
P.O. Box 25007
Denver, CO 80225

HQDA
ATTN: DAMI-POI
Washinting, D.C. 20310-1067

Mil Asst for Env Sci Ofc of
The Undersecretary of Defense
for Rsch & Engr/R&AT/E&LS
Pentagon - Room 3D129
Washington, D.C. 20301-3080

Director
Naval Research Laboratory
ATTN: Code 4110
Dr. Lothar H. Ruhnke
Washington, D.C. 20375-5000

HQDA
DEAN-RMD/Dr. Gomez
Washington, D.C. 20314

Director
Division of Atmospheric Science
National Science Foundation
ATTN: Dr. Eugene W. Bierly
1800 G. Street, N.W.
Washington, D.C. 20550

Commander
Space & Naval Warfare System Command
ATTN: PMW-145-1G (LT Painter)
Washington, D.C. 20362-5100

Commandant
U.S. Army Infantry
ATTN: ATSH-CD-CS-OR
Dr. E. Dutoit
Fort Benning, GA 30905-5090

USAFETAC/DNE
Scott AFB, IL 62225

Air Weather Service
Technical Library - FL4414
Scott AFB, IL 62225-5458

HQ AWS/DOO
Scott AFB, IL 62225-5008

USAFETAC/DNE
ATTN: Mr. Charles Glauber
Scott AFB, IL 62225-5008

Commander
U.S. Army Combined Arms Combat
ATTN: ATZL-CAW (LTC A. Kyle)
Fort Leavenworth, KS 66027-5300

Commander
U.S. Army Combined Arms Combat
ATTN: ATZL-CDB-A (Mr. Annett)
Fort Leavenworth, KS 66027-5300

Commander
U.S. Army Space Institute
ATTN: ATZI-SI (Maj Koepsell)
Fort Leavenworth, KS 66027-5300

Commander
U.S. Army Space Institute
ATTN: ATZL-SI-D
Fort Leavenworth, KS 66027-7300

Commander
Phillips Lab
ATTN: PL/LYP (Mr. Chisholm)
Hanscom AFB, MA 01731-5000

Director
Atmospheric Sciences Division
Geophysics Directorate
Phillips Lab
ATTN: Dr. Robert A. McClatchey
Hanscom AFB, MA 01731-5000

Raytheon Company
Dr. Charles M. Sonnenschein
Equipment Division
528 Boston Post Road
Sudbury, MA 01776
Mail Stop 1K9

Director
U.S. Army Materiel Systems
Analysis Activity
ATTN: AMXSY-MP (H. Cohen)
APG, MD 21005-5071

Commander
U.S. Army Chemical Rsch,
Dev & Engr Center
ATTN: SMCCR-OPA (Ronald Pennsyle)
APG, MD 21010-5423

Commander
U.S. Army Chemical Rsch,
Dev & Engr Center
ATTN: SMCCR-RS (Mr. Joseph Vervier)
APG, MD 21010-5423

Commander
U.S. Army Chemical Rsch,
Dev & Engr Center
ATTN: SMCCR-MUC (Mr. A. Van De Wal)
APG, MD 21010-5423

Director
U.S. Army Materiel Systems
Analysis Activity
ATTN: AMXSY-AT (Mr. Fred Campbell)
APG, MD 21005-5071

Director
U.S. Army Materiel Systems
Analysis Activity
ATTN: AMXSY-CR (Robert N. Marchetti)
APG, MD 21005-5071

Director
U.S. Army Materiel Systems
Analysis Activity
ATTN: AMXSY-CS (Mr. Brad W. Bradley)
APG, MD 21005-5071

Commander
U.S. Army Laboratory Command
ATTN: AMSLC-CG
2800 Powder Mill Road
Adelphi, MD 20783-1145

Commander
Headquarters
U.S. Army Laboratory Command
ATTN: AMSLC-CT
2800 Powder Mill Road
Adelphi, MD 20783-1145

Commander
Harry Diamond Laboratories
ATTN: SLCIS-CO
2800 Powder Mill Road
Adelphi, MD 20783-1197

Director
Harry Diamond Laboratories
ATTN: SLCHD-ST-SP
Dr. Z.G. Sztankay
Adelphi, MD 20783-1197

Air Force Systems Command/WER
Andrews AFB, MD 20334-5000

National Security Agency
ATTN: W21 (Dr. Longbothum)
9800 Savage Road
Ft George G. Meade, MD 20755-6000

U. S. Army Space Technology
and Research Office
ATTN: Brenda Brathwaite
5321 Riggs Road
Gaithersburg, MD 20882

OIC-NAVSWC
Technical Library (Code E-232)
Silver Springs, MD 20903-5000

The Environmental Research
Institute of MI
ATTN: IRIA Library
P.O. Box 8618
Ann Arbor, MI 48107-8618

Commander
U.S. Army Research Office
ATTN: DRXRO-GS (Dr. W.A. Flood)
P.O. Box 12211
Research Trianagle Park, NC 27709

Dr. Jerry Davis
North Carolina State University
Department of Marine, Earth, &
Atmospheric Sciences
P.O. Box 8208
Raleigh, NC 27650-8208

Commander
U. S. Army CECRL
ATTN: CECRL-RG (Dr. H. S. Boyne)
Hanover, NH 03755-1290

Commanding Officer
U.S. Army ARDEC
ATTN: SMCAR-IMI-I, Bldg 59
Dover, NJ 07806-5000

U.S. Army Communications-Electronics
Command Center for EW/RSTA
ATTN: AMSEL-RD-EW-SP
Fort Monmouth, NJ 07703-5303

Commander
U.S. Army Communications-Electronics
Command
ATTN: AMSEL-EW-D (File Copy)
Fort Monmouth, NJ 07703-5303

Headquarters
U.S. Army Communications-Electronics
Command
ATTN: AMSEL-EW-MD
Fort Monmouth, NJ 07703-5303

Commander
U.S. Army Satellite Comm Agency
ATTN: DRCPM-SC-3
Fort Monmouth, NJ 07703-5303

Director
EW/RSTA Center
ATTN: AMSEL-EW-DR
Fort Monmouth, NJ 07703-5303

USACECOM
Center for EW/RSTA
ATTN: AMSEL-RD-EW-SP
Fort Monmouth, NJ 07703-5303

6585th TG (AFSC)
ATTN: RX (CPT Stein)
Holloman AFB, NM 88330

Department of the Air Force
OL/A 2nd Weather Squadron (MAC)
Holloman AFB, NM 88330-5000

PL/WE
Kirtland AFB, NM 87118-6008

Director
U.S. Army TRADOC Analysis Command
ATTN: ATRC-WSS-R
White Sands Missile Range, NM 88002

Rome Laboratory
ATTN: Technical Library RL/DOVL
Griffiss AFB, NY 13441-5700

Department of the Air Force
7th Squadron
APO, NY 09403

AWS
USAREUR/AEAWX
APO, NY 09403-5000

AF Wright Aeronautical Laboratories
Avionics Laboratory
ATTN: AFWAL/AARI (Dr. V. Chimelis)
Wright-Patterson AFB, OH 45433

Commander
U.S. Army Field Artillery School
ATTN: ATSF-F-FD (Mr. Gullion)
Fort Sill, OK 73503-5600

Commandant
U.S. Army Field Artillery School
ATTN: ATSF-TSM-TA
Mr. Charles Taylor
Fort Sill, OK 73503-5600

Commander
Naval Air Development Center
ATTN: Al Salik (Code 5012)
Warminister, PA 18974

Commander
U.S. Army Dugway Proving Ground
ATTN: STEDP-MT-DA-M
Mr. Paul Carlson
Dugway, UT 84022

Commander
U.S. Army Dugway Proving Ground
ATTN: STEDP-MT-DA-L
Dugway, UT 84022

Commander
U.S. Army Dugway Proving Ground
ATTN: STEDP-MT-M (Mr. Bowers)
Dugway, UT 84022-5000

Defense Technical Information Center
ATTN: DTIC-FDAC
Cameron Station
Alexandria, VA 22314

Commanding Officer
U.S. Army Foreign Science &
Technology Center
ATTN: CM
220 7th Street, NE
Charlottesville, VA 22901-5396

Naval Surface Weapons Center
Code G63
Dahlgren, VA 22448-5000

Commander
U.S. Army OEC
ATTN: CSTE-EFS
Park Center IV
4501 Ford Ave
Alexandria, VA 22302-1458

Commander and Director
U.S. Army Corps of Engineers
Engineer Topographics Laboratory
ATTN: ETL-GS-LB
Fort Belvoir, VA 22060

TAC/DOWP
Langley AFB, VA 23665-5524

U.S. Army Topo Engineering Center
ATTN: CETEC-ZC
Fort Belvoir, VA 22060-5546

Commander
Logistics Center
ATTN: ATCL-CE
Fort Lee, VA 23801-6000

Commander
USATRADOC
ATTN: ATCD-FA
Fort Monroe, VA 23651-5170

Science and Technology
101 Research Drive
Hampton, VA 23666-1340

Commander
U.S. Army Nuclear & Cml Agency
ATTN: MONA-ZB Bldg 2073
Springfield, VA 22150-3198